SSCL-255

# The Superconducting Super Collider

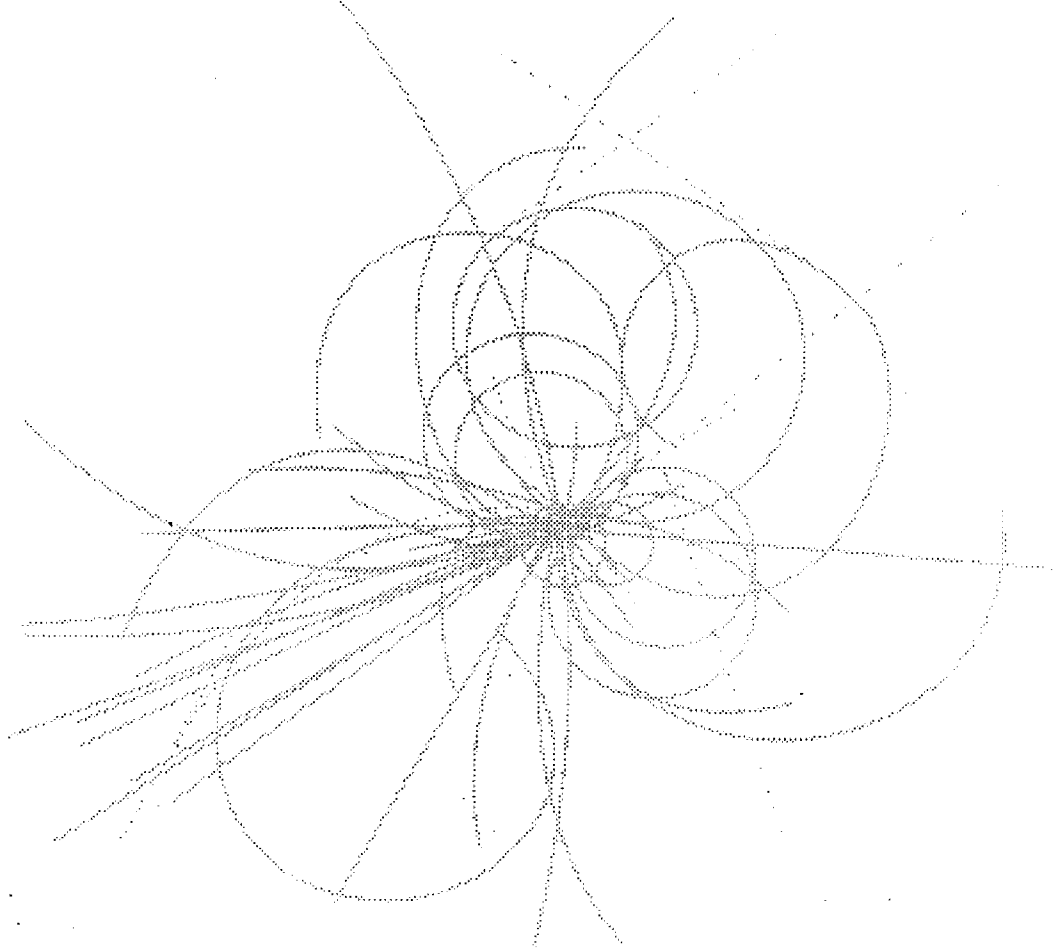

# Quench Origins


**Arnaud Devred**

**SSC Laboratory**


**March 1990**

SSCL-255

# Quench Origins*

Arnaud Devred

KEK, National Laboratory for High Energy Physics
1-1 Oho, Tsukuba-shi, Ibaraki-ken, 305, JAPAN

for the

Superconducting Super Collider Laboratory†
2550 Beckleymeade
Dallas, TX 75237

March 1990

*Lecture delivered at the*

*1989/1990 U.S. Particle Accelerator School*
*Brookhaven National Laboratory*
*Upton, New York*

*July 29-August 4, 1989*

*Work supported by the SSC Laboratory, Dallas, Texas, USA, under Contract No. SSC-90-I-02109.

†Operated by the Universities Research Association, Inc. under contract with the U.S. Department of Energy.

# QUENCH ORIGINS*

Arnaud DEVRED
KEK, National Laboratory for High Energy Physics
1-1 Oho, Tsukuba-shi, Ibaraki-ken, 305, Japan

## 1 INTRODUCTION

### 1.1 What Is a Quench?

The superconducting state only exists when materials are maintained below a temperature called the *critical temperature*. This critical temperature depends on many parameters, including the amount of current carried by the conductors, and the magnetic field on the conductors (which for a given turn of a magnet coil are of course related). A three-dimensional surface, called the *critical surface*, is defined by the boundaries of critical temperature, critical magnetic field, and critical current, as shown in Figure 1. The critical surface is the very boundary between the superconducting and normal resistive states.

A magnet is normally operated at conditions corresponding to a point located beneath the critical surface, where the entire coil is superconducting. Let us assume that starting from this operating point we ramp up the current. In ramping up the current (and thus the magnetic field) we get closer and closer to the critical surface, and soon, somewhere in the coil, we cross it. Crossing the critical surface means that somewhere in the coil a small volume of conductor, $V$, switches to the normal resistive state. When switching to the normal resistive state, this small volume dissipates power by the Joule effect. The dissipated power overheats $V$, and also, by thermal diffusion along the conductor, the region $dV$, which surrounds $V$. If the Joule heating is sufficient, $dV$ can in turn reach the critical temperature, switch to the normal resistive state, and dissipate power; the dissipated power can in turn overheat $dV$, and, by thermal diffusion, the region surrounding $dV$ — and so on. Under certain conditions, a self-maintained process can be established — from transition, to power dissipation, to thermal diffusion and then again to transition — in which the *normal zone*, the zone where the conductors have switched to the normal resistive state, *propagates* through the entire coil. This process is called a *quench*.

### 1.2 The Effects of a Quench

As described above, once a small volume of conductor has switched to the normal resistive state, it dissipates power. A fraction of this dissipated power is transferred to the surroundings of the initial volume of transition (either along the conductor, or, transversely, to the conductor insulation or the helium), but the main part is consumed locally in overheating the conductor. In a very short time (a few tenths of a second in the case of a dipole or quadrupole magnet) the conductor temperature, initially that of the helium, reaches room temperature, and, if nothing is done to discharge the current, keeps on increasing. At temperatures above 1000 K, the current capability of the superconductor begins to degrade irreversibly. At about the same temperatures, the conductor insulation (usually Kapton film) loses its strength and resistance to cut-through. A turn-to-turn short is then very likely to occur, which will severely damage the coil and render it unusable. If not controlled, the effects of a quench can thus be disastrous.

* Work supported by the SSC Laboratory, Dallas, Texas, USA, under contract No. SSC-90-I-02109.

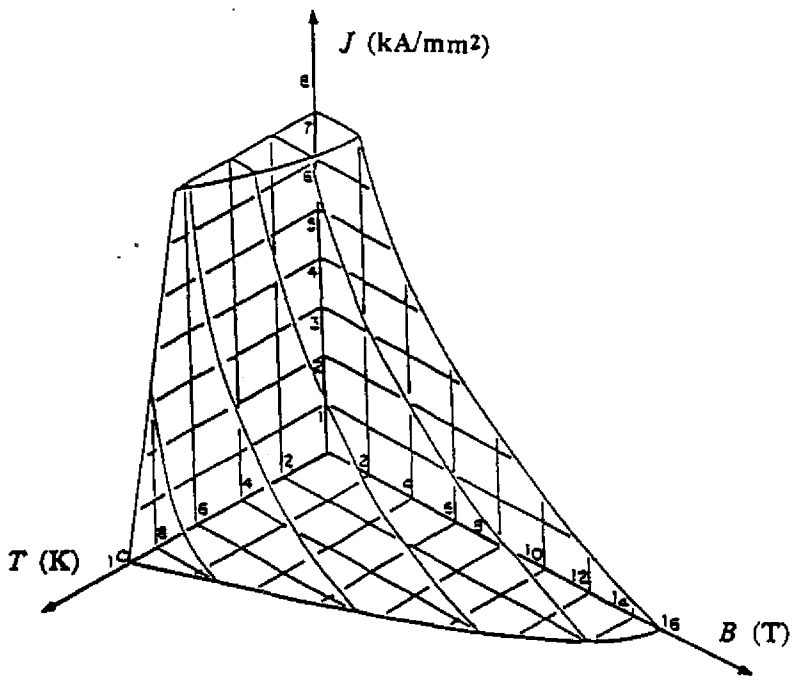


Figure 1. NbTi critical surface.

In the operation of a superconducting magnet, a quench is, of course, a disturbance. Everything must therefore be done to limit the risks of quenching. As we will see, one important factor is the position of the operating point of the magnet relative to the critical surface. Nevertheless, as much as we might limit the risks, they can never be nil. Every superconducting magnet is likely to experience quenches during its lifetime. We must therefore ensure that these quenches will not be destructive. In other words, we must ensure that the coil will not reach a temperature higher than even a fraction of 1000 K. This implies two things: 1) that we have to be able to detect quench occurrence, and 2) that we have to be able to discharge the coil and extract its stored energy quickly enough to limit the power dissipation by the Joule effect. These concerns cannot be addressed without understanding the very nature of the quench phenomenon, its origins, and its laws of propagation. This shows the importance of quench studies, which, besides fulfilling an academic interest, also answer an engineering demand.

## 1.3 Studying the Quench

My oral presentation consisted of three parts: quench origins (how and why does a quench occur), quench development (how the quench propagates through the coil), and safety concerns (how to detect a quench, how to estimate the temperature increase, and what to do to protect the coil). In this paper, however, I shall only discuss the quench origins, sending the reader to references 1 to 3, which contain experimental data from the testing of 4-cm aperture, 17-m long SSC dipole prototypes, for supplementary information on quench development and magnet safety.

As for the quench origins, I shall first establish a method of classification and introduce the notions of *conductor-limited* and *energy-deposited* quenches (paragraph 2). Paragraph 3 will be devoted to the study of conductor-limited quenches, and I shall introduce the notions of *plateau* and of *fraction of short sample*. Paragraph 4 will be devoted to the study of energy-deposited quenches, and I shall introduce the notions of *training* and of *minimum energy deposit*; I shall then review the possible causes of energy release. Lastly, in paragraph 5, I shall introduce the notion of *operating margin*, and I shall indicate how to optimize the operating margin in order to limit the risk of premature quenching.

## 2 QUENCH CLASSIFICATION[4]

### 2.1 Definitions

Let us consider a superconducting coil wound with a conductor of known critical current $I_C\,(T, B)$. At a given current, the magnetic field on the conductor is variable from turn to turn, and also, for a given turn, from the inner edge to the outer edge of the conductor. Let $B = f_p(I)$ designate the relation between the current and the maximum magnetic field seen by the conductor in the coil, also called the *peakfield*. At a given temperature, $T_0$, the maximum current, $I_{max}$, that can circulate in the coil is the solution of the implicit equation

$$I = I_C\,(T_0, f_p(I)) \qquad \text{at } T_0. \tag{1}$$

When ramping up the current from zero, quenches can occur either at currents lower than $I_{max}$, or as $I_{max}$ is reached; this provides a first classification of the quenches.

The quenches occurring at $I_{max}$ are a consequence of the intrinsic characteristics of the conductor, and nothing can be done about them except to improve the conductor. I shall call these *conductor-limited quenches*. The other quenches are different in nature. Since they occur at a current, $I$, lower than $I_{max}(T_0)$, somewhere in the coil a volume of conductors is subject to a temperature increase, $T_0 + \Delta T$, such that

$$I \geq I_{max}(T_0 + \Delta T) \quad . \tag{2}$$

These quenches are therefore initiated by a deposit of energy on the conductor. I shall call them *energy-deposited quenches*. Thus, the main difference between the conductor-limited and the energy-deposited quenches is that in conductor-limited quenches the critical surface is crossed because of an increase in current, while in energy-deposited quenches the critical surface is crossed because of a local increase in temperature.

### 2.2 Identification Method[5]

The above definitions rely on knowing $I_C\,(T, B)$. As we shall see in paragraph 3.2, the transition from the superconducting to the normal resistive state is much more complicated than a single-step function, and in practical applications $I_C(T, B)$ is not very well defined and ought to be measured on each particular conductor. Nevertheless, the sorting of the quenches into conductor-limited and energy-deposited categories remains relevant, and is of great interest for the magnet builder since it gives him direct information on what is limiting the performance of the magnet. I shall now set forth a method which allows clear categorization of quenches, independent of the numerical values of $I_C\,(T, B)$.

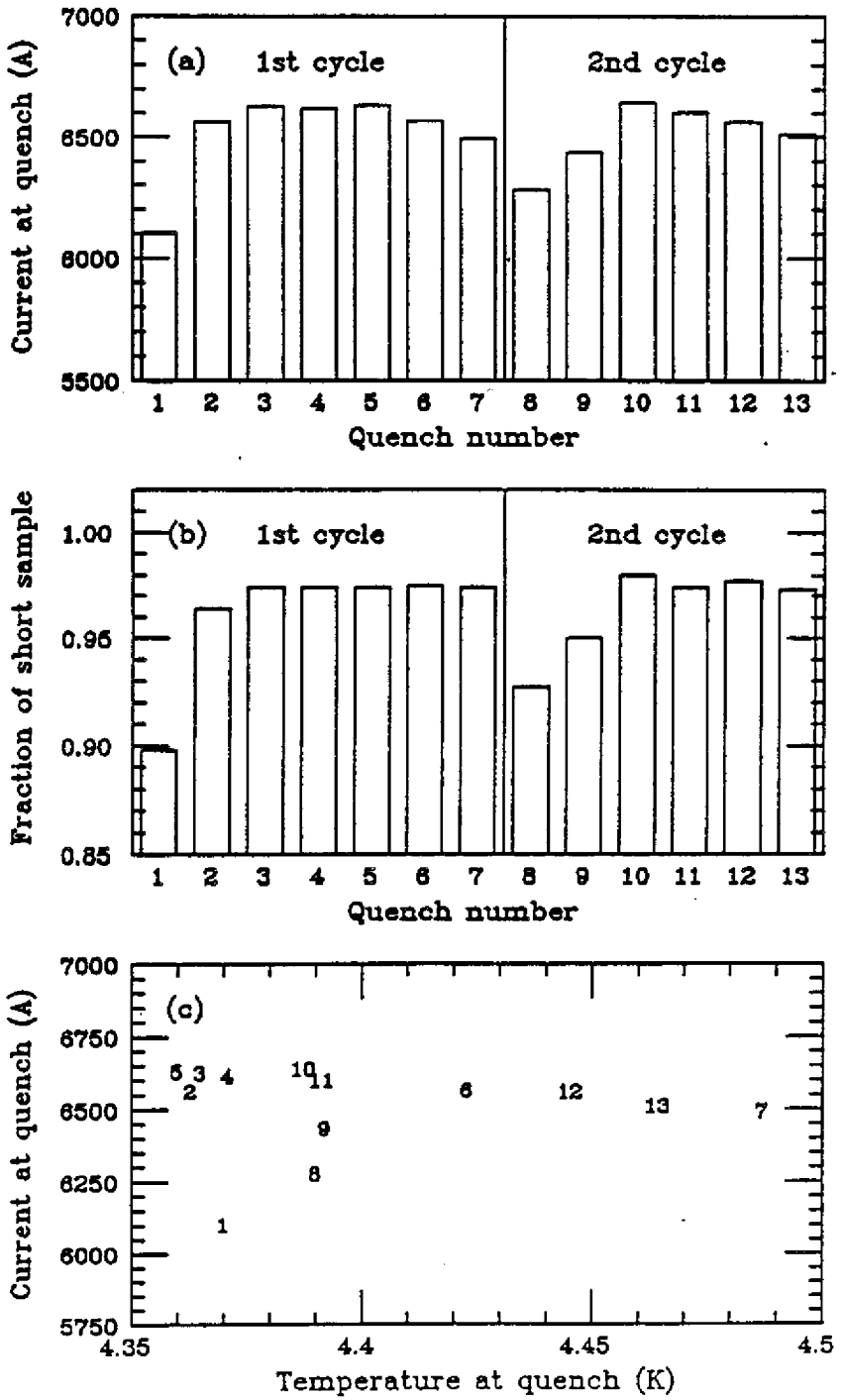


Figure 2. Selected testing results from SSC dipole prototype DD0017. (a) Current at quench versus quench number. (b) Fraction of short sample vs. quench number. (c) Current at quench vs. temperature at quench.

Let us assume that the operating temperature of the magnet is changed from $T_0$ to $T_0 + \Delta T_0$. In the case of conductor-limited quenches, the current at quench will change from $I_{max}(T_0)$ to $I_{max}(T_0 + \Delta T_0)$; there will be a strong correlation between the current at quench and the operating temperature, closely following the critical surface of Figure 1. On the other hand, for energy-deposited quenches, the deposit of energy presumably has nothing to do with the fine tuning of the magnet temperature. Instead, as we shall see in paragraph 4.3, it is more likely due to a stress relief or a friction between wires resulting from the energization of the magnet and the application of strong Lorentz forces. If Lorentz forces are involved, it is therefore expected that the energy-deposited quenches should depend mainly on the current level and should be relatively insensitive to small variations in temperature. Thus a practical method for categorizing quenches is to change the operating temperature of the magnet slightly — for example, to increase it and then decrease it by 50 mK — and to see if the quench current follows the change or not.

### 2.3 Practical Example

Figures 2a and 2c feature an illustration of the method set out above. These results are extracted from the excitation test of a 4-cm aperture, 17-m long SSC dipole prototype (magnet DD0017).[6-9] The magnet was first cooled down to a nominal temperature of 4.4 K, and ramped several times to quench. A "ramp to quench" consists of ramping the magnet current until a quench occurs; the power supply is then switched off and the coil is discharged. Following the quench, the magnet is cooled down again to 4.4 K, and the test is repeated. In this particular case, the magnet was quenched seven times and then warmed up to room temperature for several days. It was then cooled down again to 4.4 K, and six more quenches were taken. Figure 2a shows the current at quench versus the quench number, and Figure 2c shows the current at quench versus the magnet temperature. (The temperature is measured by carbon resistors located in the helium interconnect region at both extremities of the magnet.) Quenches 3 to 7 and 10 to 13 exhibit a clear correlation between the current and the temperature, while quenches 1, 2, 8, and 9, the first two quenches of each test cycle, are scattered; thus quenches 1, 2, 8, and 9 are energy-deposited quenches, while the others are conductor-limited quenches.

## 3 STUDY OF CONDUCTOR-LIMITED QUENCHES

### 3.1 The Notion of Plateau

As we have seen, conductor-limited quenches can be characterized by their strong dependence on temperature. On the other hand, if the temperature of the magnet is kept constant, the current level at which conductor-limited quenches occur is very stable. In the plot of the current at quench versus the quench number, these quenches appear on a "plateau"; they are called *plateau quenches*. When testing a superconducting magnet, the operating temperature is deliberately kept constant. The first sign of a conductor-limited quench is thus the appearance of a plateau in the current-at-quench plot. Once this plateau has been clearly established, one can verify that these quenches are indeed conductor-limited by deliberately varying the operating temperature, as recommended in paragraph 2.2. This is the procedure that has been followed for the magnet in Figure 2a, and this is why the last quenches of the testing cycles, which were taken at slightly higher temperatures, seem to fall off the plateau.

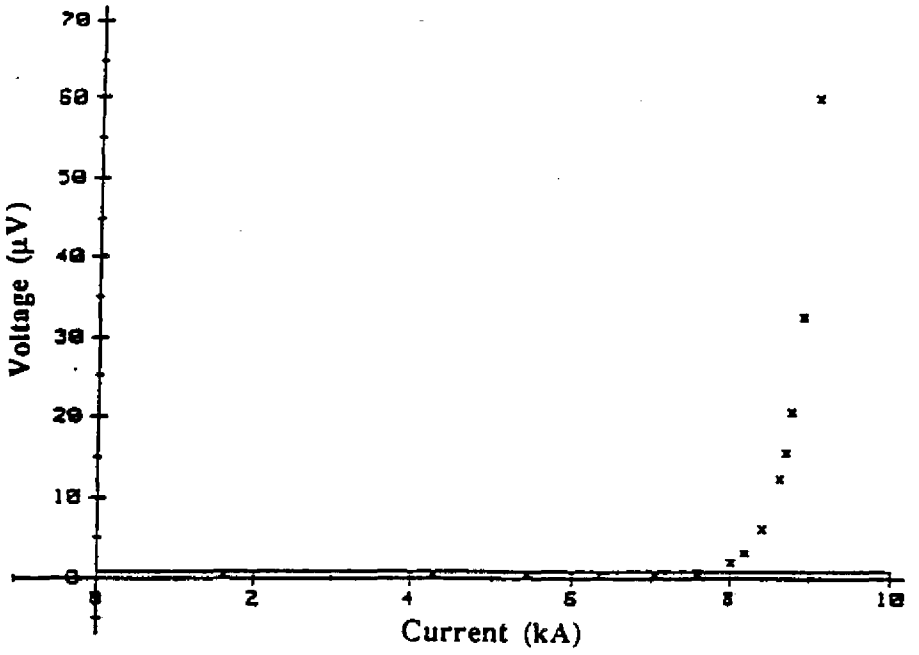


Figure 3. Voltage-current characteristic of an SSC inner-layer conductor (at 4.33 K and 6 T).

An important consequence of conductor-limited quenches is that they reveal the maximum current that can be put into the coil. This means that, in the operation of a magnet, once a plateau has been reached, there is no hope of improving the performance except by deliberately lowering the operating temperature. This also means that a correlation like the one in Figure 2c provides an *in situ* measurement of the conductor critical current. The next step, then, is to compare these *in situ* values with the critical current previously anticipated for the conductor wound in the coil. Before we can make this comparison, however, we must understand how the critical current of a conductor is defined, and how the maximum current of Eq. (1) can be predicted.

### 3.2 Defining the Critical Current

The conductors currently used in accelerator magnets are typically a couple of millimeters thick and 1-cm wide. They consist of 20 to 40 strands wound in a spiral pattern. Each strand consists of a large number (typically 1000) of small (typically 10 μm in diameter), twisted, superconducting filaments, embedded in a copper matrix.[10] In this highly complex structure, the transition from the superconducting to the normal resistive state is not abrupt, as is clear from Figure 3, which shows the voltage-current characteristic of a 75-cm long sample of SSC conductor at a temperature of 4.33 K and in a background magnetic field of 6 T.[11] For low currents, no voltage is measured, indicating that the whole sample is superconducting. For currents above 7000 A, a finite voltage appears, indicating that part of the current is no longer carried by superconducting electrons. As we keep increasing the current, this voltage increases rapidly, and finally the whole sample switches to the normal resistive state at a current, $I_t$, of about 9000 A.

The curvature of the $U$–$I$ characteristic of the sample is not well understood, and is influenced by many parameters, including the filament size and the magnetic field.[12,13] It is usually represented by the equation

$$\rho_a = \frac{UA}{IL} = \text{const}\, I^n \qquad \text{for } I < I_t, \tag{3a}$$

where $\rho_a$ is the apparent resistivity of the sample, $A$ and $L$ are the cross-sectional area and the length of the sample, and n is an integer, called the *N-value*. The N-value is inversely related to the width of the $U$–$I$ curvature and is used to characterize the quality of the transition from the superconducting to the normal resistive state. (A "bad" conductor has an N-value of less than 10, while a "good" conductor has an N-value of 30 or more.) Of course, when the current exceeds $I_t$, the apparent resistivity is the resistivity of the conductor in the normal state

$$\rho_a = \frac{1+r_{CuS}}{r_{CuS}}\rho_{Cu} \qquad \text{for } I > I_t, \tag{3b}$$

where $r_{CuS}$ is the conductor's copper-to-superconductor ratio.

Since the transition is not abrupt, the value of the critical current is not accurately determined, and many ways to define a *pseudo* critical current present themselves. The most commonly-used standard[12] is to define the critical current $I_C$ as the current value at which the apparent resistivity defined in Eq. (3a) is equal to $10^{-14}$ Ωm

$$\rho_a(I_C) = 10^{-14} \qquad \text{at } T \text{ and } B. \tag{4}$$

This is the definition we shall use throughout the paper. Also, since the manipulation of Eqs. (3a) and (3b) is mathematically complex, we shall sometimes idealize the conductor transition by representing the apparent resistivity by the step function

$$\rho_a = \Upsilon(I - I_C(T, B))\,\frac{1+r_{CuS}}{r_{CuS}}\rho_{Cu} \qquad \text{at } T \text{ and } B, \tag{5}$$

where Υ is the Heaviside step function.

### 3.3 Generating the Critical Surface

Because the critical current defined in Eq. (4) depends on the temperature and on the magnetic field, in order to entirely determine the critical surface the conductor sample should be tested under varying $T$ and $B$, and for each value of $(T, B)$ a characteristic similar to the one in Figure 3 should be drawn, and the N-value and $I_C$ measured. This, however, is rather tedious and very expensive. To avoid this, many studies have been carried out to determine a parametrization of the critical surface — that is, an analytical representation of the critical surface that can be adapted to each particular conductor by measuring only a few characteristics.[14,15] In the case of the SSC conductor, the most appropriate parametrization (in the range: $4.0 < T < 4.5$ K and $5 < B < 8$ T) has been found to be[16]

$$I_C(T,B) = \left(1 + \frac{-0.315319\ u - 0.01528\ u^2 + 0.00161\ u^3}{1 - 0.163089\ v}\right)$$

$$\times \left(\frac{1 - 0.231741\ v}{1 - 0.021249\ v - 0.020418\ v^2}\right) I_C(4.2\ \mathrm{K}, 5\ \mathrm{T}), \quad (6)$$

where $u = T - 4.2$, $v = B\ \ 5$, and $I_C(4.2\ \mathrm{K}, 5\ \mathrm{T})$ is the critical current at 4.2 K and 5 T. In this parametrization, the critical surface of a conductor can thus be entirely generated from the measured value of the critical current at 4.2 K and 5 T.

### 3.4 Short-Sample Current Prediction

Before winding a superconducting coil, a sample of conductor is taken from the spool, and is tested in a specific test setup in order to measure its critical characteristics. In the case of the SCC conductor, one tries to measure with as much accuracy as possible the value of $I_C$ at 4.2 K and 5 T.[17] With the use of Eq. (6), this allows an estimate of the critical current for all $T$ and $B$. Introducing this $I_C(T, B)$ into Eq.(1) then allows one to predict the maximum current that can be put into the magnet. (The peakfield function $f_p$ only depends on the geometry of the magnet coil, and can be easily calculated using any of the existing computer codes.)[18] This maximum current, derived from the critical current measured on a *short sample* of conductor, is called the *short-sample current prediction*, and is usually noted $I_{ss}$. Note that $I_{ss}$ only depends on the operating temperature $T_0$.

### 3.5 Fraction of Short Sample

As we noted in paragraph 3.1, the interesting fact about conductor-limited quenches is that they provide an *in situ* measurement of the conductor critical current once it has been wound into a coil. It now seems appropriate to compare these values with the short sample predictions.

By definition, the *fraction of short sample* of a quench is the ratio $\eta$

$$\eta = \frac{I_q}{I_{ss}(T_0)} \quad , \qquad (7)$$

where $I_q$ is the current at quench, $T_0$ is the temperature at quench, and $I_{ss}$ is the short-sample current prediction for $T_0$. If $\eta$ equals one, the quench is called a *short-sample quench.*[*]

### 3.6 Degradation or Not Degradation?

Let us return to the example of the SSC dipole prototype in paragraph 2.3 (magnet DD0017). The parameters of the inner-layer conductor are listed in Table 1, and the peakfield function is given by

$$f_p(I) = 0.7505 + 0.9470\ 10^{-3}\ I \quad . \qquad (8)$$

---

[*] Since the transition from the superconducting to the normal resistive state is not abrupt, and since the definition of $I_C$ is somewhat arbitrary, the fraction of short sample may at times exceed 1.

Table 1. Selected Parameters of the Inner-Layer Conductors of SSC Dipole Prototypes

| | Specifications[19] | DD0017 | DD0019 |
|---|---|---|---|
| Number of Strands | 23 | 23 | 23 |
| Strand Diameter (mm) | 0.808 | 0.808 | 0.808 |
| Copper-to-Superconductor Ratio | 1.3 | 1.59 | 1.44 |
| Copper RRR | 70 | 70 | 80 |
| $I_C$(4 2 K,5 T) (A) | 14097 | 12848 | 12076 |
| $I_{ss}$(4.35 K) (A) | 7006 | 6820 | 6691 |

Figure 2b shows a plot of the fraction of short sample versus the quench number. For quenches 3 to 7 and 10 to 13, which we identified as conductor-limited quenches, the fraction of short sample appears very stable, with an average value $\eta_a$

$$\eta_a = 0.975 \quad .$$

The maximum current at which the magnet can be operated, at a nominal temperature of 4.4 K, is therefore 97.5% of the short-sample current prediction; one could also say that the current capability of the conductor has apparently been *degraded* by a factor of 3.5% compared with the short-sample predictions. The question now is whether that degradation is real, resulting for instance from bad treatment of the conductor during the coil winding, or whether it is simply due to errors in the fraction of short sample calculations.

Errors in the fraction of short sample predictions have two principle sources: 1) the inaccuracy of the critical surface parametrization itself, and 2) the inaccuracy of the temperature-at-quench measurements. In both cases, the inaccuracies can be estimated to be around 2-3%. It follows that the inaccuracy of the fraction of short sample is around 5%. If the average fraction of short sample for the plateau quenches is less than 0.95 we can then answer with confidence that the conductor has been degraded; but if $\eta_a$ is within a few percent of 1, as for the example presented above, the question remains unresolved.

As is often the case in physics when a question cannot be resolved because of inaccuracies, a solution is to rely on statistics. Indeed, if the short-sample current is always measured in the same way, in the same test setup, and if the temperature at quench is always measured with the same temperature sensors, at the same locations, the errors mentioned above should be fairly reproducible from magnet to magnet. Testing a certain number of similar magnets would then allow us to empirically define a *working* fraction of short sample, $\eta_w$, which will give the correct ratio between the "observed" plateau current and the "predicted" short-sample current. It then remain to compare $\eta_a$ and $\eta_w$: either $\eta_a$ is less then $\eta_w$, in which case the conductor can be considered as having been degraded, or $\eta_a$ is greater or equal to $\eta_w$, in which case the magnet can be considered as having reached its full performance. (Unfortunately, I do not have enough information to reliably define $\eta_w$ for the above example.)

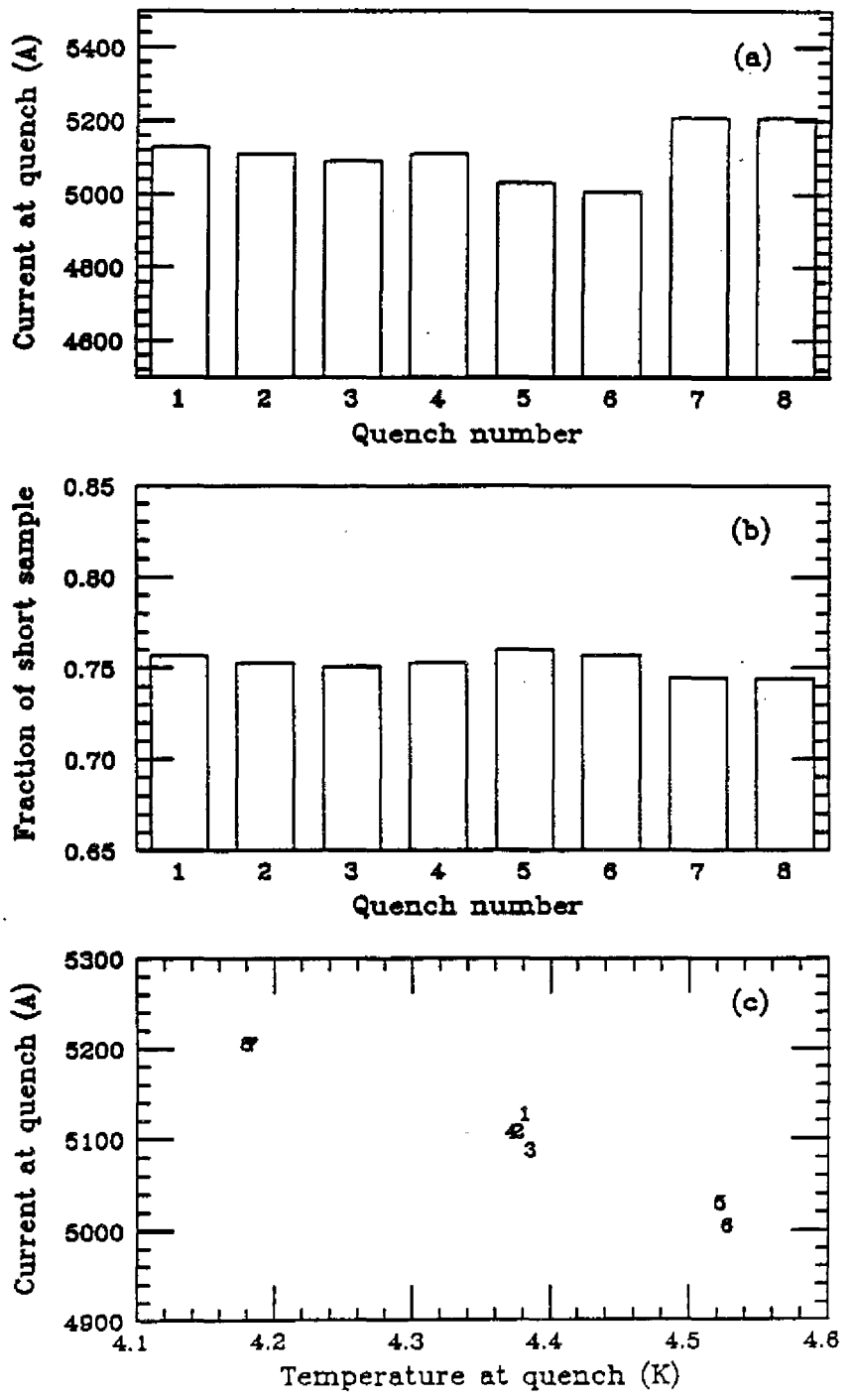


Figure 4. Selected testing results from SSC dipole prototype DD0016. (a) Current at quench versus quench number. (b) Fraction of short sample vs. quench number. (c) Current at quench vs. temperature at quench.

### 3.7 Practical Example

In actual state-of-the-art cable manufacturing and coil winding, the conductor degradation is usually less than 10%. If a magnet appears limited to fractions of short sample of less than 90%, the first move of the magnet testers is then to think of problems other than the conductor. To conclude this section I want to give another example which shows that conductor-limited quenches can indeed occur at very low fractions of short sample. This also shows that our identification criterion based on the current-at-quench versus temperature-at-quench correlation is a much more powerful tool to diagnose the magnet problems than the sole consideration of the value of the fraction of short sample.

Figures 4a to 4c summarize the testing of another 4-cm aperture, 17-m long SSC dipole prototype (magnet DD0016).[6-9] The current plot shows a neat plateau, and the temperature plot shows a strong correlation between the current and the temperature at quench. Although the average fraction of short sample is relatively low,

$$\eta_a = 0.753 \quad ,$$

these quenches exhibit all the characteristics of conductor-limited quenches. On the other hand, the magnet was equipped with voltage taps, which allow one to locate where the quench starts in the coil.[1] The analyses of the voltage data showed that all the quenches were originating in the same area. After the testing, the magnet was taken apart, and in the area identified as the quench origin it was found that each of the 23 strands in the cable contained a cold weld, resulting from an error in cable manufacturing. All the quenches were therefore initiated because of this conductor degradation, and were indeed *conductor-limited* quenches.

## 4 STUDY OF ENERGY-DEPOSITED QUENCHES

### 4.1 The Notion of Training

As we have seen, energy-deposited quenches, as opposed to conductor-limited quenches, appear scattered when their currents are plotted versus temperature. On the other hand, even if the magnet temperature is kept constant, the current level at which the energy-deposited quenches occur can vary. When testing a superconducting magnet, it is quite frequently observed, as illustrated in Figure 2a, that for the first few quenches the current at quench progressively increases, until it reaches the plateau described in paragraph 3.1. This gradual improvement of the magnet's performance is called the magnet's *training*, and these first few quenches, which precede the establishment of the plateau, are called *training quenches*.

Of course, the training can be seen in a positive light, for it leaves the hope that, even if the first quenches of a magnet are below the short-sample limit, the performance may improve and the magnet may finally reach the design current. Nevertheless, it is not reasonable to build an accelerator with several hundred or more superconducting magnets that need to be trained each time they are put into operation (or at least, each time they are warmed up to room temperature). If the magnet prototypes exhibit some training, the origin of this training has to be understood, and the design of the magnet has to be modified in order to eliminate, or at least limit, the training quenches to levels well above the operating current of the accelerator.

The study of energy-deposited quenches has two main goals: 1) to determine the amount of energy that can trigger a quench, and 2) to understand the mechanisms in a magnet coil which can release such an energy. Paragraph 4.2 will be devoted to a discussion of the *critical energy*, that is, of the minimum energy deposit which at a given temperature and current can trigger a quench, and paragraph 4.3 will review the possible *quenching disturbances*, that is, the mechanisms which, during the energization of a magnet, can release an energy larger than the critical energy.

## 4.2 Evaluating the Critical Energy

### 4.2.1 Introduction

4.2.1.1 Definitions. Let us consider a magnet coil initially in the superconducting state at a temperature $T_0$ and carrying a current $I$, and let us assume that an energy $W$ is deposited on a volume $V$ of the coil. Common sense tells us that if $W$ and $V$ are small, the diffusion along the conductor or the transfer to the helium will carry away much of the heat, so that the disturbance will progressively disappear and the whole coil will recover the superconducting state. On the other hand, if $W$ and $V$ are large, the cooling capabilities of the conductor will be exceeded, and a quench will begin. In other words, a quench can only be triggered if $W$ and $V$ are greater than certain minimum values, which I shall note $W_{CI}$ and $V_{CI}$. These qualitative results are very well verified experimentally.[20,21] $W_{CI}$ is called the *critical energy* or *minimal energy deposit*, and $V_{CI}$ is called the *minimum propagating zone*.

4.2.1.2 Calculating the Critical Energy. The calculation of $W_{CI}$ and $V_{CI}$ is a very difficult problem since it requires the solution of the three-dimensional heat-balance equation of the coil, which, besides its complex geometry, is an anisotropic medium whose properties depend non-linearly on the temperature. Practically, one must therefore do some simplifications on both the coil geometry and the material properties. Throughout the years, two main configurations of coils have been studied: the *potted magnets*, for the which the amount of helium in contact with the conductor is negligible, and the *liquid-helium bathed magnets*, for which each individual conductor is closely surrounded by helium. For the potted magnets, the heat balance equation can be written

$$C(T)\frac{\partial T}{\partial t} = \text{div}\,(\overline{\overline{k}}(T)\ \text{grad}\ T) + P_J(T) + \frac{1}{V}\frac{dW}{dt} \quad , \tag{9}$$

where $C$ is the specific heat per unit volume of conductor ($Jm^{-3}K^{-1}$), $\overline{\overline{k}}$ is a second-order tensor whose components are the thermal conductivity coefficients ($Wm^{-1}K^{-1}$), $P_J$ is the Joule heating rate per unit volume ($Wm^{-3}$), and ($dW/dt$) is the power deposit (W) which is only non-nil inside the volume $V$. For the helium-bathed magnets, each conductor can be treated independently from the others. Considering a straight conductor of z-axis and assuming that the temperature is uniform in each section, the heat balance equation can be written

$$C(T)\frac{\partial T}{\partial t} = \frac{\partial}{\partial z}(k(T)\frac{\partial T}{\partial z}) + P_J(T) - \frac{P_{He}(T)}{A} + \frac{1}{V}\frac{dW}{dt} \quad , \tag{10}$$

where $A$ is the cross-sectional area of the conductor, $k$ the longitudinal thermal conductivity, and $P_{He}$ the heat-transfer rate per unit length to the helium ($Wm^{-1}$).

Starting from these basic equations, one can either seek a quick evaluation, which will give the order of magnitude of the minimum energy deposit, or one can be more thorough and seek an exact solution. The quick evaluation consists of determining the stationary solutions $T_s$ of Eqs. (9) or (10) (that is the solutions of the steady-state equations derived from Eqs. (9) or (10) by taking $\partial/\partial t = 0$), and then defining the minimum energy deposit as the difference in enthalpy between $T_0$ and $T_s$ integrated over the coil volume

$$W_{CI} = \int\int\int_{\text{coil volume}} dV \int_{T_0}^{T_s} dT\, C(T) \qquad \text{At } I. \tag{11}$$

References 22 and 23 treat potted magnets in this way and achieve simple formulae, while references 24 and 25 consider the case of helium-bathed magnets but require a computer calculation. Complete solutions of time-dependent Eqs. (9) and (10) can only be derived numerically. References 26 to 29 deal with helium-bathed magnets. The case of potted magnets can be derived from reference 27 when the heat-transfer coefficient to the helium tends towards zero, while references 30 and 31 provide approximate solutions for the time-dependent Eq. (9) which lead to results qualitatively comparable to those of reference 23. Reference 32 presents a variation on non-uniformly bathed magnets, where only one side of the conductor is in contact with the helium, and for which Eq. (10) has to be rewritten taking into account the transverse diffusion through the conductor cross section (this study seeks to describe the coil configuration of the ISABELLE dipole). Lastly, Reference 33 studies the effect of the curvature in the $U$-$I$ characteristic of the conductor described in paragraph 3.2, but using a representation different from the N-power function of Eq. (3a).

4.2.1.3 Measuring the Critical Energy. Numerous experiments have been undertaken in order to measure $W_{CI}$ and to verify the previous theories. In most of the cases the energy is deposited by means of a small electric heater glued onto the conductor and powered by a capacitor bank or by pulsed current. The experiment consists of firing the heater with increasing voltage charge or current pulse and determining the minimum electrical energy $Q_e$ that can cause a quench. However, a non-negligible part of the electrical energy is consumed in heating both the electrical insulation between the heater and the conductor and the heater itself (or it is transferred to the coolant), so that only a fraction of $Q_e$ is actually deposited on the conductor. To derive the correct value of $W_{CI}$, one must therefore evaluate the energy losses, which present a not-so-trivial problem. References 34 to 36 provide measurements on a conductor sample, references 37 and 38 on a model solenoid, and reference 39 on an ISABELLE dipole prototype.

Another way of modeling an energy deposit, which avoids the losses in the insulator or the coolant, consists of depositing the energy by means of induction heating. As we described in paragraph 3.2, the conductor contains a large fraction of copper. One can thus think of winding a small wire around a delimited section of conductor, which, powered by a fast pulse of current, will generate a high-frequency magnetic field along the conductor axis and induce transverse eddy currents in the copper. The problem is then to calculate the Joule heating resulting from these eddy currents; this can be done relatively easily for a cylindrical conductor geometry. Measurements by this technique can be found in references 40 and 41.

4.2.1.4 Limiting Our Ambitions. As I have tried to show in this introduction the estimation of the critical energies and of the minimum propagating zones constitutes a complex question, widely debated in the literature, and yet without any definite answers. This is not the place to discuss the details of this problem, nor to try to synthesize all the studies mentioned above, although references 42 and 43 already provide very broad reviews. I shall thus content myself with a very simple approach, which will lead me to simple formulae and allow me to introduce some basic notions. However, some of the simplifying assumptions on which these calculations lay can be partially justified, and it is my belief that the results achieved are of the right order magnitude. (These results will be lengthily exploited in paragraph 5.2 in order to study the parameter influencing the magnet reliability.) The presentation I make here is largely inspired by reference 44.

4.2.2 Critical Temperature at a Given Current

Let us one more time consider a magnet coil initially in the superconducting state at a temperature $T_0$ carrying a constant current $I$, such that

$$I < I_{max}(T_0) \quad .$$

As we have described in paragraph 2.1, a quench can be triggered in the coil if the temperature in a small volume of the conductor increases to $T_0 + \Delta T$, such that

$$I \geq I_{max}(T_0 + \Delta T) \quad . \qquad (2)$$

At current $I$, the minimum temperature increase, $\Delta T_{min}$, that can trigger a quench is thus given by

$$I = I_{max}(T_0 + \Delta T_{min}) \quad . \qquad (12)$$

Let us define the *critical temperature at current I*, $T_{CI}$, as

$$T_{CI} = T_0 + \Delta T_{min} \qquad \text{at } I. \qquad (13)$$

Replacing $I_{max}$ in Eq. (12) by its definition shows that, at a given current, $T_{CI}$ is the solution of the implicit equation

$$I = I_C(T, f_p(I)) \qquad \text{at } I. \qquad (14)$$

From this definition, the minimum energy that can trigger a quench thus appears to be that required to overheat the conductor from $T_0$ to $T_{CI}$. A critical energy per unit volume of conductor, $E_{CI}$, can thus be defined by

$$E_{CI}(T_0,I) = \int_{T_0}^{T_{CI}} dT\ C(T) \qquad (\mathrm{Jm^{-3}}), \qquad (15)$$

where $C$ is the specific heat per unit volume of conductor.

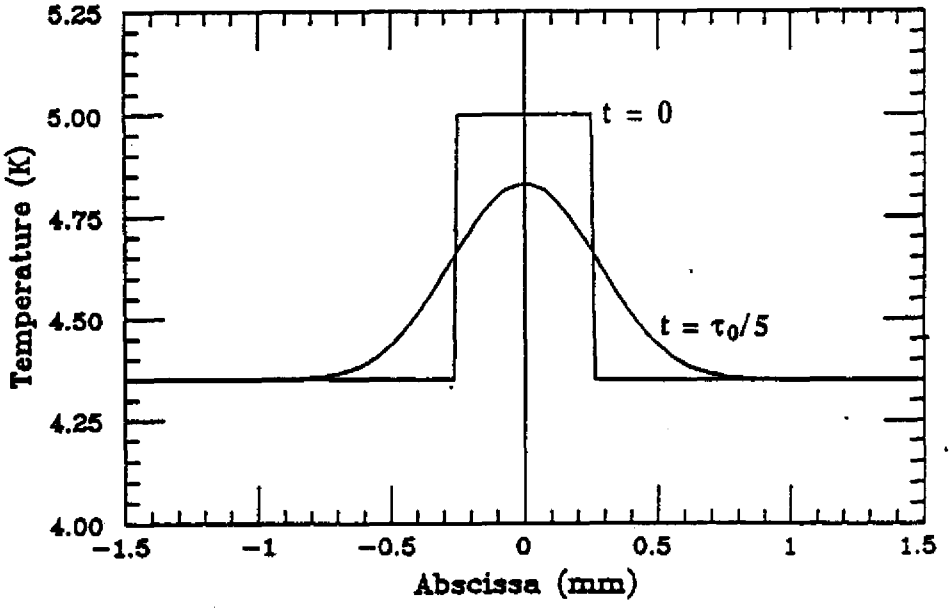


Figure 5. Diffusion of a thermal disturbance.

4.2.3 Minimum Propagating Zone

Let us now consider a given turn of the magnet coil and let us assume that, at $t = 0$, an instantaneous disturbance overheats uniformly to $T_{CI}$ a length $l$ of conductor.* Let us idealize the conductor transition to the normal resistive state by Eq (5); when switching to the normal resistive state the conductor thus starts to dissipate a power density $P_J$

$$P_J = \rho \left(\frac{I}{A}\right)^2 \qquad (\mathrm{Wm^{-3}}), \qquad (16)$$

where $\rho$ is the conductor resistivity in the normal state and $A$ is the conductor's cross-sectional area.

During the first instants following the disturbance, the main thermal phenomenon is the diffusion along the conductor of the initial sawtooth of temperature, as illustrated in Figure 5. Assuming that the conductor behaves adiabatically, it can be shown that this sawtooth progressively flattens with a characteristic time $\tau_0$[45]

$$\tau_0 = \frac{l^2}{2\,D_{th}} \quad , \qquad (17)$$

where $D_{th} = k/C$ is the conductor's thermal diffusivity ($\mathrm{m^2s^{-1}}$) and $k$ is the conductor's thermal conductivity.

* An instantaneous deposit of energy $W_0$ can be introduced in Eqs. (9) and (10) by replacing $(\partial W/\partial t)$ with $\delta(t)W_0$ where $\delta$ is the Dirac function.

The diffusion of the initial thermal disturbance is then relayed to the Joule heating, and the main thermal phenomenon becomes the quench propagation. The time $\tau_q$ needed to initiate a quench can be evaluated by considering the rate at which $P_J$ is consumed in overheating the superconducting zone from $T_0$ to $T_{CI}$, that is

$$\tau_q = \frac{E_{CI}}{P_J} \quad . \tag{18}$$

Of course the relay in question must take place if a quench is to occur. This means that the initial sawtooth must not vanish before the quench propagation has begun. In other words, a quench can only be triggered if

$$\tau_0 > \tau_q \quad . \tag{19}$$

It follows that the length of the initial disturbance must be such that

$$l > l_{CI} = \sqrt{\frac{2\, D_{th}\, E_{CI}}{P_J}} \quad . \tag{20}$$

If the initial disturbance is longer than $l_{CI}$, a quench will be triggered; if the initial disturbance is shorter than $l_{CI}$, the normal zone will collapse and the conductor will recover the superconducting state. $l_{CI}$ is thus the length of the minimum propagating zone defined in paragraph 4.2.1.1. (In our model of uniform disturbance over the conductor cross section, the volume $V_{CI}$ is simply $A\, l_{CI}$.)

4.2.4 Minimum Energy Deposit.

The last step of our calculations is simple. From the definitions of $E_{CI}$ and $l_{CI}$, it follows that, at a given operating temperature and at a given current, the minimum energy deposit that can trigger a quench is

$$W_{CI}(T_0, I) = E_{CI}\, A\, l_{CI} = \sqrt{\frac{2\, D_{th}}{\rho}}\, \frac{E_{CI}^{3/2}\, A^2}{I} \quad , \tag{21}$$

where, in the numerical applications, we shall take the value of $D_{th}$ at $T_{CI}$.

4.2.5 Practical Example.

To illustrate these calculations, let us consider the case of the 4-cm aperture, 17-m long SSC dipole prototype DD0019.[8-9] The parameters of the inner-layer conductor wound in this magnet are listed in Table I. The peakfield function of the magnet is that of Eq. (8). The material properties at cryogenic temperatures of copper and niobium titanium are given in the Appendix. For $T_0$ = 4.35 K and $I$ = 6500 A (the operating point of the current SSC design), we get

$$T_{CI} = 4.52\ \text{K}, \quad E_{CI} = 477\ \text{Jm}^{-3}, \quad l_{CI} = 436\ \mu\text{m}, \quad W_{CI} = 2.5\ \mu\text{J}.$$

According to these calculations, a few micro-Joules deposited on half a millimeter of conductor are thus sufficient to trigger a quench!

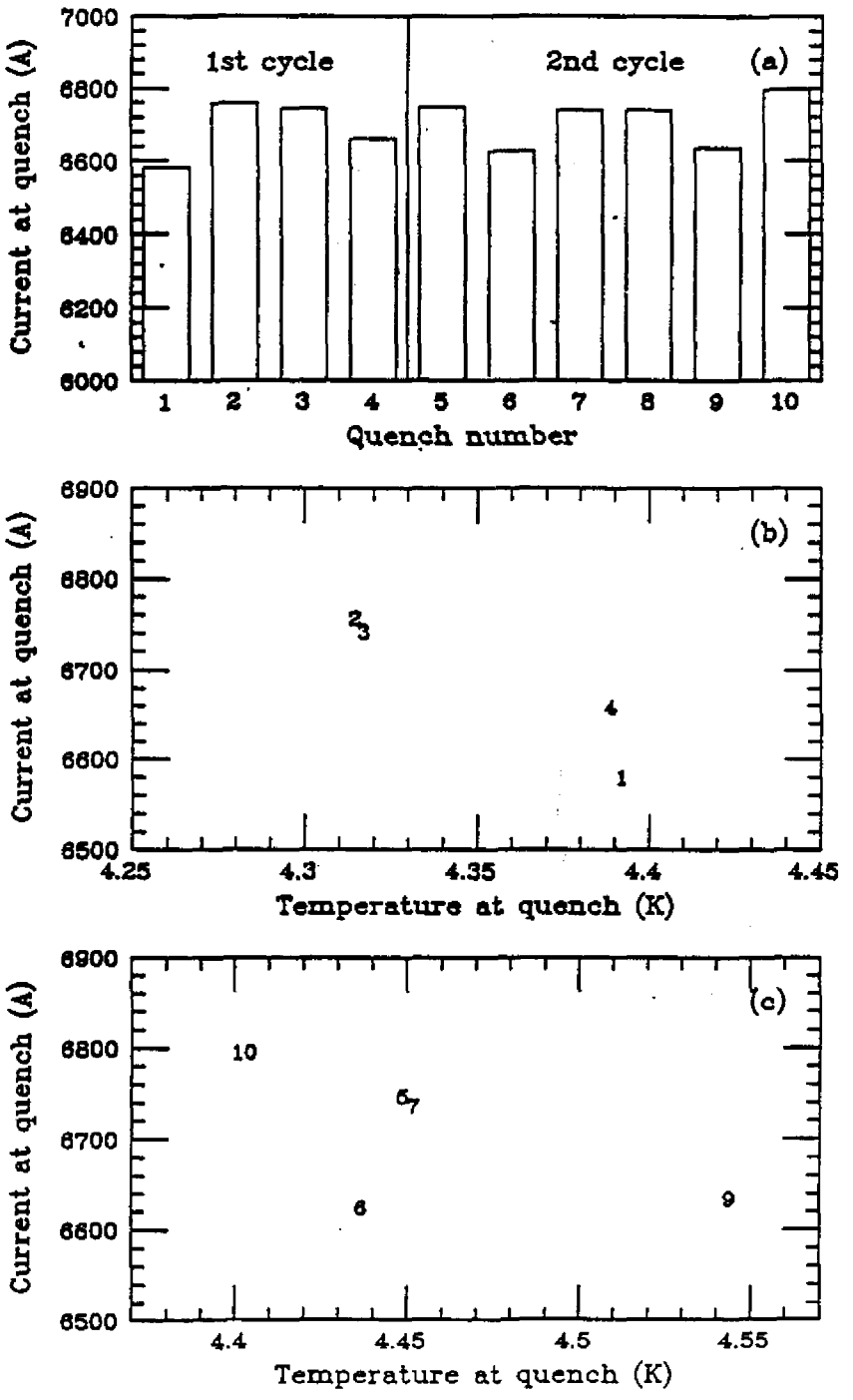


Figure 6. Selected testing results from SSC dipole prototype DD0019. (a) Current at quench versus quench number. (b) Current at quench vs. temperature at quench (1st testing cycle). (c) Current at quench vs. temperature at quench (2nd testing cycle).

The interesting thing about magnet DD0019 is that it provides a mean to evaluate the actual disturbances that occur in such a magnet. Like for magnet DD0017, the testing included two cycles separated by a warm-up to room temperature. The two cycles were done following the same procedure: the magnet was first cooled down to a nominal temperature of 3.5 K, and ramped up and down several times from zero to a maximum current of 6800 A; it was then warmed up to a nominal temperature of 4.35 K, and ramped to quench as described in paragraph 2.3. For both cycles, the magnet reached 6800 A at 3.5 K without quenching; the current-at-quench plots for the subsequent testings at 4.35 K are given in Figures 6a to 6c. (The current-at-quench versus temperature-at-quench data are presented on two separate plots, because the offsets and the gains of the temperature signal amplifiers were accidentally changed between cycles. The temperature for quench 8 is missing.) Figures 6b and 6c show that two of the quenches were energy-deposited — quenches 1 and 6.

These two energy-deposited quenches at 4.35 K occurred at a current level of 6500-6600 A, which is less than the 6700-6800 A reached during the preliminary *conditioning* at 3.5 K. Since all the other parameters were kept constant (including the current ramp rate, 16 $As^{-1}$) the only difference was the operating temperature, and thus the critical energy. It follows that the energy release, $Q$, at the origin of these quenches is such that

$$W_{CI}(4.35\ \mathrm{K}, 6500\ \mathrm{A}) < Q < W_{CI}(3.5\ \mathrm{K}, 6700\ \mathrm{A}) \quad .$$

With the numerical data for DD0019, this becomes

$$2.5\ \mu\mathrm{J} < Q < 16.7\ \mu\mathrm{J} \quad .$$

The energy release that triggered quenches 1 and 6 was thus of the order of 10 μJ. This is also the order of magnitude of the critical energies measured in References 37 and 38 for the high values of fraction of short sample.

### 4.2.6 Limits of the Calculation

In the course of the above calculation, we introduced a certain number of assumptions, which limit the validity of our results. They are: 1) that the conductor transition can be represented by a step function at temperature $T_{CI}$, 2) that the conductor behaves adiabatically, and 3) that the energy deposit was instantaneous and uniform over the conductor cross section. I shall now try to justify, at least partially, some of these assumptions.

4.2.6.1 Transition Temperature. The selection of the temperature at which the transition "really" happens is an important parameter, for a variation of a few tenths of a degree in the upper limit of the integral defining $E_{CI}$ could greatly influence the result. An indirect verification that $T_{CI}$ is the right choice can be done as follows. We have seen that a characteristic time $\tau_q$ of the quench propagation could be defined by Eq. (18). Let us make $T_0$ tend towards $T_{CI}$; it follows that $E_{CI}$ and thus $\tau_q$ tend towards zero. This predicts that for $T_0$ tending towards $T_{CI}$, which is equivalent to $I$ tending towards $I_{ss}(T_0)$, or the fraction of short sample tending towards 1, the quench tends to propagate infinitely rapidly. On the other hand, if we can verify experimentally that the quench tends to propagate infinitely rapidly when the fraction of short sample tends towards 1, this would provide a proof that $I_{ss}(T_0)$ or $T_{CI}$ are the thresholds that "really" matter in the transition. Reference 2 present measurements of the quench propagation velocities in the SSC dipole prototypes; it appears that both the longitudinal

velocity (along the conductor) and the transverse velocity (from turn to turn) increase dramatically when the fraction of short sample tends towards 1. Although these velocities remain measurable, they reach values that can be qualified as quasi-infinite at the scale of the "usual" thermal phenomena.

4.2.6.2 Hypothesis of Adiabaticity. The second assumption consisted of admitting that, at the time scale of the quench initiation, the conductor could be regarded as behaving adiabatically. In other words, we assumed that the amount of heat transmitted to the conductor's surroundings during the time $\tau_q$ was negligible. An indirect verification of this assumption can be done by comparing $\tau_q$ to the turn-to-turn propagation time $\tau_{t\text{-}to\text{-}t}$, that is, to the time needed for the heat to diffuse from the actual conductor to its neighbors and to switch them to the normal resistive state. The data on the transverse propagation given in reference 2 show that for the whole range of fraction of short sample

$$\tau_{t\text{-}to\text{-}t} \geq 2.5 \text{ ms} \quad .$$

On the other hand, for magnet DD0019 at 4.35 K and 6500 A (same calculations as in paragraph 4.2.5), we get

$$\tau_q = 2 \ \mu\text{s} \quad .$$

These two times thus differ by several orders of magnitude, which can prove that not much heat is transferred outside the conductor during the time of the quench initiation.

4.2.6.3 Geometry of the Energy Deposit. The last hypothesis deals with the geometry of the energy deposit and is probably the most questionable. Indeed, we assumed that the energy was uniformly deposited on the whole conductor cross section. However, as we shall see in the next paragraph, a quench can be caused by the motion of a single strand, or because of a small crack or a debonding in the resin impregnated in the conductor. The energy released by such disturbances, involving a couple of strands and their neighbors, is thus only deposited on a fraction $fA$ of the conductor cross section, and has yet to diffuse through the remaining $(1-f)A$. A characteristic time $\tau_{tr}$ of the transverse thermal diffusion is given by

$$\tau_{tr} = \frac{(1-f)^2 A^2}{D_{tr} P_d^2} \quad , \tag{22}$$

where $P_d$ is the diffusion perimeter, that is the perimeter of $fA$ in contact with $(1-f)A$, $D_{tr} = k_{tr}/C$ is the transverse thermal diffusivity of the conductor, and $k_{tr}$ is the transverse thermal resitivity of the conductor. Evaluating $k_{tr}$ is not a simple problem; however, since the thermal conductivity of niobium titanium is very small, $k_{tr}$ is certainly less than the thermal resistivity of copper $k_{Cu}$

$$k_{tr} \leq k_{Cu} \quad . \tag{23}$$

Let us assume an energy deposit on 4 strands of magnet DD0019 conductor, and let us take for $P_d$ the thickness of this conductor (1.6 mm). We get

$$D_{tr} \leq 0.070 \text{ m}^2\text{s}^{-1} \qquad \text{and} \qquad \tau_{tr} \geq 529 \ \mu\text{m}.$$

The time $\tau_{tr}$ appears very large compared to the time $\tau_q$ calculated from the uni-dimensional model. We should thus redo the calculation of the critical energy starting from Eq. (9), taking into account the transverse thermal diffusion. This, of course, is a significant problem, but one which largely overreaches the framework of this presentation. I shall therefore stop here, assuming in the following that the orders of magnitude of $l_{CI}$ and $W_{CI}$ given by Eqs. (20) and (21) remain valid, even if the energy is deposited on a fraction of the conductor cross section. (Clues on how to treat the three-dimensional problem can be found in references 23, 30, and 32. Some experimental investigations of the effect of the conductor size can also be found in references 46 and 47.)

## 4.3 Possible Training Causes

### 4.3.1 Introduction

Three mechanisms can be envisioned as responsible for sudden energy releases when ramping up the current in a magnet and thus applying strong Lorentz forces: 1) frictional heating due to wire motion, 2) failures in the epoxy impregnation, and 3) microyielding in the niobium titanium. Since these causes are all of mechanical nature, we shall call the quenches they trigger *mechanically-induced quenches*. As we shall see shortly, mechanically-induced quenches seem to be the best explanation of magnet training, and though for the purpose of clarity I shall now discuss each cause separately, giving, when possible, some indication of how to limit their occurrence, we should bear in mind that the training of a real magnet results from a mixture of the three. The presentation given here is largely inspired from reference 48. (Energy releases can, of course, also result from the development of a short between two turns of a coil, or between the coil and its mechanical support, but the discussion of such topics is not suitable to an academic presentation....)

### 4.3.2 Wire Motions

4.3.2.1 Training Model. The first cause of training to have been identified was frictional heating due to wire motions.[49] As described in paragraph 3.2, the conductors used in accelerator magnets are made of several strands twisted together, with a compaction factor of about 90%. This leaves 10% of unfilled space, along with many interfaces between the strands, where sliding can occur. In addition, the conductor is helically wrapped with several layers of insulation. The twist pitch of the inner layers of insulation is usually small to allow overlapping and to ensure good electrical insulation, but the twist pitch of the outer layer is usually larger, leaving a channel between turns for helium circulation. This is illustrated in Figure 7, which depicts the insulation scheme of the SSC conductor. Thus in the conductor insulation there are also mechanical tolerances and many interfaces where sliding can occur.

When energizing the magnet, strong Lorentz forces are applied to the conductor strands and are then transmitted to the mechanical supports through the insulation. In a geometry as complex as that of a dipole coil, there are many interfaces in a friction configuration, that is, where the Lorentz force has a tangential component. One can therefore imagine that, at some current level, somewhere in the coil, a static-friction coefficient is exceeded so that sliding can occur which, if inelastic, dissipates heat. If the heat dissipation exceeds the critical energy, a quench can then be triggered.

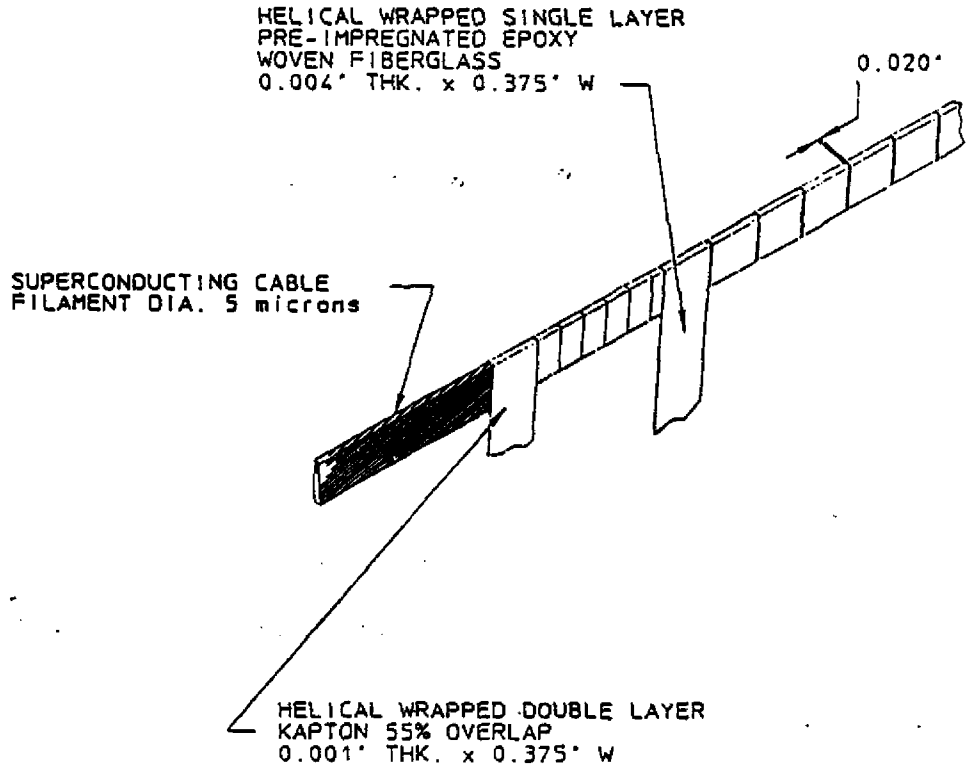


Figure 7. Current insulation scheme of the SSC dipole conductor.

One can also imagine that the strand or conductor motion responsible for the quench has put the strand or the conductor in a better position, so that during the subsequent energization, the distribution of the Lorentz force in that region is improved, and the same current level can be reached without exceeding the static-friction coefficient. In this case the current can be increased until, somewhere in the coil, another static-friction coefficient is exceeded, which can in turn provoke a frictional motion large enough to trigger a quench — and so on. Quench after quench the current level would increase until it reaches the critical current. This is one possible explanation for magnet training.

As was described above, the interfaces where friction can occur are strand-to-strand and conductor-to-insulator. Of course, the physics of the phenomena taking place at these interfaces is much more complicated than the single static-friction coefficient we evoked. In fact, in the case of the conductor-to-insulator interface, it has been shown that the macroscopic *creep* is preceded by so-called *microslips*, which occur at the microscopic scale when the shear stress locally exceeds the yield stress of the softer material (here, the insulator), provoking plastic flows.[50,51] The energy released by these microslips is believed to be sufficient to induce a quench.[52,53] Further investigations of the role of friction can be found in reference 54, while references 55 and 56 study the effects of the insulation spacing.

4.3.2.2 Evaluating the Energy Release. The Lorentz force, $F$, on one strand of conductor, of length $l$, is

$$F = \frac{I\,B\,l}{m} \quad , \tag{24}$$

where $m$ is the number of strands in the conductor. Let us assume that the strand moves a distance $\delta$ against friction, so that the work heats the conductor. The energy deposit $Q$ on the conductor is therefore

$$Q = \frac{I\,B\,l}{m}\delta \quad . \tag{25}$$

This deposit can only trigger a quench if

$$Q \geq W_{CI} \quad . \tag{26}$$

The minimum wire motion $\delta_{min}$ that can trigger a quench is thus

$$\delta_{min} = \frac{m}{I\,B}\frac{W_{CI}}{l_{CI}} \quad . \tag{27}$$

Let us now consider the actual specifications for the SSC dipole inner-layer conductor listed in Table 1 ($m$ is 23), and let us take for $B$ the peakfield value given by Eq. (8). We saw in paragraph 4.2.5 that at 4.35 K and 6500 A the minimum energy deposit was of the order of 10 μJ on half a millimeter of conductor. We get

$$\delta_{min} = 10\ \mu m.$$

At the operating conditions, a frictional displacement of 10 μm of one strand of the conductor is thus enough to trigger a quench!

Of course, this calculation is very crude and should not be regarded as a precise solution. First, the Lorentz force is not perpendicular to the conductor, but also has a tangential component; the equations describing the turn equilibrium are thus more complicated than the single radial projection considered above.[57] Also, we assumed that all the energy was transformed into heat, when actually part of it is consumed in *bending* the wire (it would thus be more more correct to speak of *wire bending* instead of wire motion.[55]) However, it is our belief that the order of magnitude given by Eq. (27) is correct. (We shall see in paragraph 5.2.2 another way to evaluate the size of the quenching disturbances from the mechanical energy stored in the coil.)

4.3.2.3 Preventing Wire Motions. We are thus faced with the imperative task of limiting the risk of wire motions. Two paths present themselves. First is that of resin (epoxy) impregnation, which would serve as a glue to prevent sliding, and would also both enhance the coil's rigidity and allow it to be assembled in one block. However, as we shall see in the next paragraph, epoxy resin, because of its brittleness at low temperatures, introduces a new source of quenching which is thought to be even less controllable than wire motion. Therefore, in modern accelerator magnets, epoxy impregnation is restricted to the minimum necessary for coil assembly, and great care is taken to limit the epoxy's contact with the conductor.

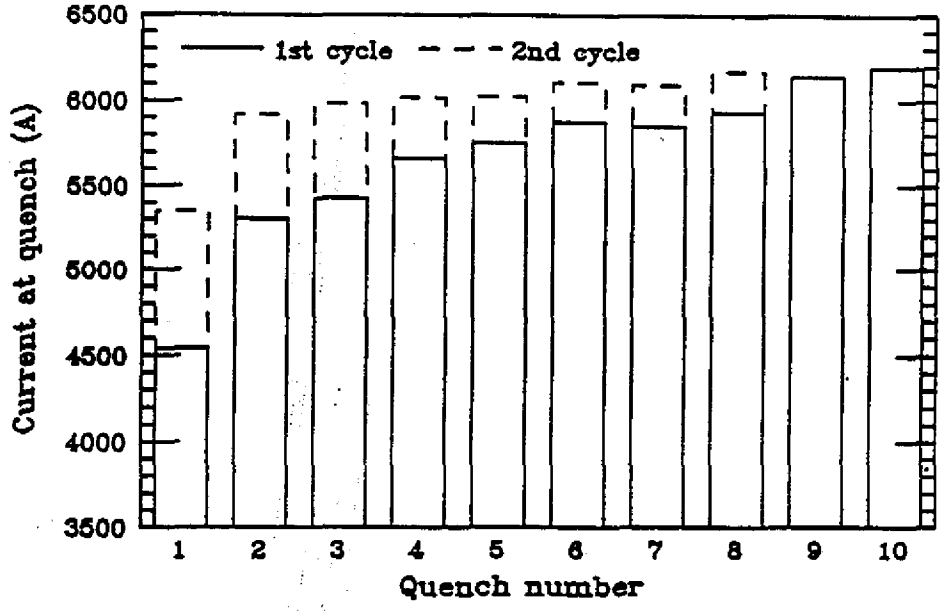


Figure 8. Selected testing results from SSC dipole prototype SD501/01.

The second, more effective, path to prevent sliding is to hold the conductor as tight as possible. This is realized by clamping the coil inside a very rigid structure and, at room temperature and zero current, making the structure exert onto the coil a compressive load greater than the expansive load produced by the Lorentz force during energization. This is called *prestressing* the coil. A complete description of this technique can be found in reference 58, so here I shall limit myself to one illustration of how prestressing can improve the training performances.

A 5-cm aperture, 1-m long SSC model dipole (magnet SD501/01)[59,60] was first built and tested with relatively low prestress on the inner coil, estimated at 10 to 20 MPa at room temperature. It was then taken apart, and rebuilt, using the same superconducting coil, collar packs and iron laminations, but increasing the prestress on the inner coil (by adjusting some shims at the pole) to a measured value at room temperature of 70 to 80 Mpa. Figure 8 shows the results of the excitation tests (the magnet was tested in a vertical dewar and the temperature is assumed to be constant, 4.2 K). In the first test (low prestress), it took 6 to 8 quenches to reach the operating current of 5980 A. In the second test (high prestress), the operating current is reached on the second quench and a relatively stable plateau is reached on the 5th quench. One can conclude from these results that by dramatically increasing the prestress, the conductors are better secured and less inclined to move. One ought to keep in mind, however, that the prestress cannot be indefinitely increased, first because it decreases the voltage breakdown of the insulation, and second because it increases the risk of microslips. An optimum must therefore be found.

### 4.3.3 Epoxy Failures

4.3.3.1 Training Model. As we have seen, the first means considered to prevent the conductors from moving was to impregnate the coil with resin, the most commonly used being epoxy. However it was soon discovered that the epoxy resin itself could be the source of a quench.[61] Indeed, the epoxy resin becomes brittle at low temperatures, that is, it has a relatively low toughness fracture, in both tension and shear. In addition, there is a difference of a factor of four in the integrated thermal contraction from room temperature to 4.2 K between the epoxy and the conductor. When an impregnated coil is cooled down, it is thus very likely that microfractures occur in the resin. Furthermore, when the coil is energized, these microfractures become stress-concentration sites, along with other spots, arising from the complex Lorentz force distribution. One can imagine that, at a certain level of current, somewhere in the resin, the stress exceeds a critical value, producing a crack (fracture in the bulk of the resin) or a debonding (failure at the interface between the resin and a conductor strand). If the energy released by the failure exceeds the critical energy, a quench can be triggered.[62-66]

On the other hand, once the crack or the debonding has occurred, the stress concentration at the point where the quench originated has been relieved. During the next energization, the same level of current can therefore be reached without producing any failure. The current can then be increased until, somewhere in the resin, another critical value of stress is exceeded, which provokes an energy release large enough to trigger a quench — and so on. This is another possible explanation for the magnet training.

4.3.3.2 Evaluating the Energy Release. Let $\sigma$ designate the average stress in the resin, and $Y$ its young modulus. The elastic energy $Q$ that can be released by a crack of volume $V$ is

$$Q = \frac{1}{2}\frac{\sigma^2}{Y} V \quad . \tag{28}$$

If we assume that this energy is entirely deposited on the conductor, the minimum crack volume $V_{min}$ that can trigger a quench is

$$V_{min} = 2\frac{Y\, W_{CI}}{\sigma^2} \quad . \tag{29}$$

Given $V_{min}$, a critical thickness of epoxy coating, $e_c$, can be defined by

$$e_c = \frac{V_{min}}{\pi\, d\, l_{CI}} \quad , \tag{30}$$

where $d$ is the strand diameter.

Let us consider the case of magnet DD0019. The strand diameter is 0.808 mm, and the average stress on the inner layer at 6500 A is around 35 MPa.[6-9] With the young modulus of the epoxy at helium temperature K being 8 GPa,[67] we get

$$V_{min} = 0.065 \text{ mm}^3 \qquad \text{and} \qquad e_c = 60\ \mu\text{m}.$$

An epoxy film of 60 μm thickness coated on the conductor strands is therefore capable of triggering a quench!

As in paragraph 4.3.2.2, this calculation should not be taken as a precise solution. First, as we have noted, the failures occur at particular and usually accidental sites of stress concentration, and it is this local stress maximum that should be introduced in Eq. (28). Of course we have no means to predict these values. In addition, we assumed that all the released energy was transformed into heat, when part of it is consumed in enlarging the crack.[68] However, it is one more time our belief that this calculation gives the correct orders of magnitude. (It will indeed serve as model for the generalization we shall develop in paragraph 5.2.2).

4.3.3.3 Preventing Epoxy Failure. Several methods can be envisioned to limit the risks of failure in the impregnation. One might first think of using a resin which has a low tensile strength, like oil or wax, which will store less elastic energy to be released in the case of a crack.[69] However, these materials have a long-term durability problem and cannot be used in practical applications. One might then think of a solution opposite to the previous one, which would be to strengthen the impregnating resin. This can be done by co-winding the conductor with a fiberglass cloth, which also plays the role of crack arrester,[70-72] a technique which is now widely used. Another school of thought is to let the superconducting coil, as a whole body, move freely inside its mechanical support in order to avoid the stress concentrations which result from strong clamping.[73-76] Nevertheless, even if they bring substantial improvements, none of these methods entirely eliminates the risks of cracking or debonding. In the case of the SSC, it has therefore been decided to adopt a low profile and to limit the use of epoxy to what is needed for coil assembly, and also to avoid direct contact between the epoxy and the conductor. This has led to the insulation scheme described in paragraph 4.3.2.1 and shown in Figure 7, where a barrier of two layers of kapton is interposed between the conductor and the pre-impregnated fiberglass. It is to be noted, however, that investigations are still under way to better understand the mechanism of these epoxy cracks and debondings.[77,78]

4.3.4 Niobium Titanium Microyielding

Even if the two previous possible causes of training could be entirely elimated, there would still remain a source of training, this time inherent to the superconductor itself. Indeed it has been known for a long time that the conductor short samples, like those we described in paragraph 3.4 which are tested in specific test setups, exhibit a training similar to that of the coil, whatever cautions are taken in their preparation.[79,80] This short-sample training is more than ever observed on today's fine-filament conductors.[81] Reference 82 explains the short-sample training by the discontinuous yielding, or serration, of the nobium titanium, whose elastic limit has been locally exceeded. (The serration is a general phenomenon among metals at low temperatures, which occurs in the plastic range, and consists of sudden drops in the stress-strain curve resulting from local softening of the material.) The local plastic deformations of the niobium titanium, where the serration can take place, can, for instance, be induced by fractures or intermetallic inclusions at the surface of the filaments.[83] A model describing this microyielding and an estimate of the energy release are derived in references 84 and 85. A solution to this problem has been to strain-cycle the conductor at room temperature up to strain levels corresponding to the serration range of niobium titanium at 4. 2 K (about 1%).[82,86,87] No experiment of this kind has yet been conducted on the SSC conductor.

## 4.4 Investigating Premature Quenching

Let us now adopt the point of view of the magnet builder. When testing a magnet prototype, the first concern is to determine if the magnet can reach the design current and be reliably operated at that current without quenching. Of course, in the R&D phase of an accelerator this is rarely achieved on the first trial, and the SSC dipole prototypes cited above are no exception. It means that the original magnet design has to be improved, and the only scientific ground from which to figure out what improvements are needed is to understand the causes of *premature quenching*. To achieve this understanding two kinds of information are needed: 1) information about the quench-start locations, and 2) information about the causes of the quench.

A very successful technique to localize the quench start is to instrument the model magnet coil with a large number of voltage taps. In the case of the 17-m long SSC dipole prototype the quench start can be located within 10 cm, and, for most quenches, obvious correlations between the spots designated as quench-start locations and conductor defaults or mechanical weaknesses have been found, subsequently leading to major design improvements.[1] However, one ought to be fair and point out that the installation of the voltage taps is time-consuming, and that they undoubtedly create a risk of shorts.

To determine what causes the quench, we must first discriminate between conductor-limited and energy-deposited quenches as described in paragraph 2.2. If we find that the quench is energy-deposited, then it remains to discriminate between the possible causes outlined in paragraph 4.3. Of course, in some cases, the knowledge of the quench-start location will be enough to determine the quench cause. Nevertheless, two more systematic methods can be used to experimentally determine the origin of mechanically-induced quenches; in fact they yield their best results when run in tandem. These are, first, to analyze the voltage fluctuations and, second, to analyze the acoustic emissions of the magnet coil during energization.

Indeed, these two methods have long been used in training studies, and it has long been known that the energization of a magnet, or even of a short sample of conductor, is accompanied by bursts of acoustic emission and that the voltage across the magnet or the short sample exhibits spikes.[88,89] Early studies showed that the frequency and the intensity of the acoustic emissions increased with the current, and that the quench was often preceded by a strong acoustic burst or voltage pulse.[89] It was then discovered that the rate of emission was reduced after the first few energizations.[90-92] These acoustic emissions or voltage fluctuations were finally related to wire motions or impregnation failures in the superconducting winding.[93-98]

The fact that mechanical disturbances produce acoustic emissions is a general property of materials and is not specific to superconducting magnets. The spikes that appear in the voltage, however, need some more explanation.[99] In a coil wound with today's twisted multifilamentary conductor, they are indeed thought to be the signature of wire movement. Let us consider a strand of length $l$ moving a distance $dx$ over a time $dt$. This generates across the strand a voltage pulse $U$

$$U = B\, l \frac{dx}{dt} \quad , \tag{31}$$

where $B$ is the magnetic field on the strand. This voltage pulse is of course very brief, and thus appears as a spike in the coil voltage.

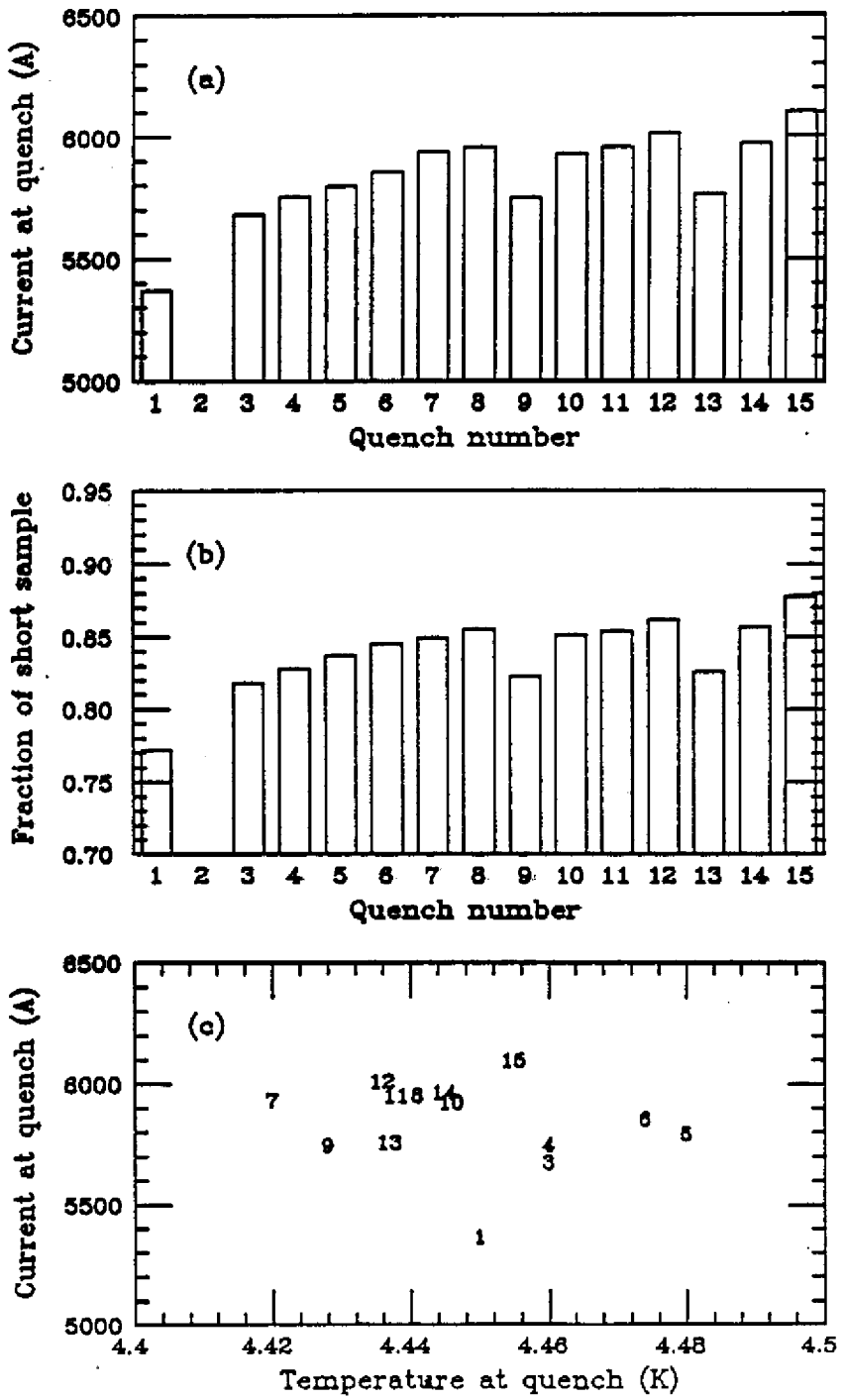


Figure 9. Selected testing results from SSC dipole prototype DD0010. (a) Current at quench versus quench number. (b) Fraction of short sample vs. quench number. (c) Current at quench vs. temperature at quench.

If a spike in the coil voltage can be interpreted as a wire motion, an idea of the energy $Q$ released by the disturbance is given by

$$Q = \int_{\text{under spike}} dt\, U\, I \quad . \tag{32}$$

This provides an *in situ* measurement of the mechanical disturbance. However, the coil voltage, especially during energization, picks up many other inductive components which, in order to make sense of the previous calculations, have to be considered, rendering the analysis relatively difficult. Some interesting results on an insertion quadrupole prototype for TRISTAN can nevertheless be found in reference 100.

As we just saw, a wire motion induces a spike in the coil voltage. On the other hand, an epoxy crack will not induce any severe voltage fluctuation. Monitoring simultaneously acoustic emissions and coil voltage then allows one to classify the quenches into three categories: 1) quenches preceded by an acoustic emission burst and a voltage spike, 2) quenches preceded by an acoustic emission burst, but without a voltage spike, and 3) quenches with neither an acoustic emission burst nor a voltage spike. Class-1 quenches can be interpreted as wire-motion induced quenches, class-2 quenches can be interpreted as epoxy-crack induced quenches, and class-3 quenches as conductor-limited quenches.[94] Examples of quench origin analyses made by monitoring acoustic emission and coil voltage can be found in references 100 to 103.

## 4.5 Practical Example

To conclude this section I want to give another example which shows that a magnet does not necessarily train, that is, that it can exhibit a succession of energy-deposited quenches which are not accompanied by an improvement in current performance. This is the case of the 4-cm aperture, 17-m long SSC dipole prototype DD0010,[6,104,105] whose testing results are presented in Figure 9a to 9c. (The data for quench 2 are missing.) Figure 9a shows that the current at quench never reached a stable plateau, and Figure 9b shows that the fraction of short sample remained low. The ultimate proof that these quenches were indeed energy-deposited is given by Figure 9c where the current at quench and the temperature at quench appear unrelated.

Whereas up until now we have seen that energy releases that initiate mechanically-induced quenches can, at least locally, improve mechanical stability and allow larger currents to be reached for subsequent quenches, one can also imagine that if the mechanical instability at the quench origin is too large, the conductor will move to and fro, or multi-cracks might occur (or even propagate!) in the epoxy, so that mechanical stability is never achieved. This is exactly what happened in magnet DD0010. As for the other 17-m long SSC dipole prototypes, DD0010 was equipped with voltage taps.[1] The voltage tap data showed that all the quenches were originating in the same turn of the inner coil, but at different locations along the magnet. When disassembling the magnet it was found that the copper wedge mounted next to that turn (for reasons of field quality) was misaligned, leaving a large gap for the conductor to move (the wedge literally fell off onto the floor during the uncollaring of the coil). That particular turn of the coil was thus not secured enough, and could move without ever finding a stable position.

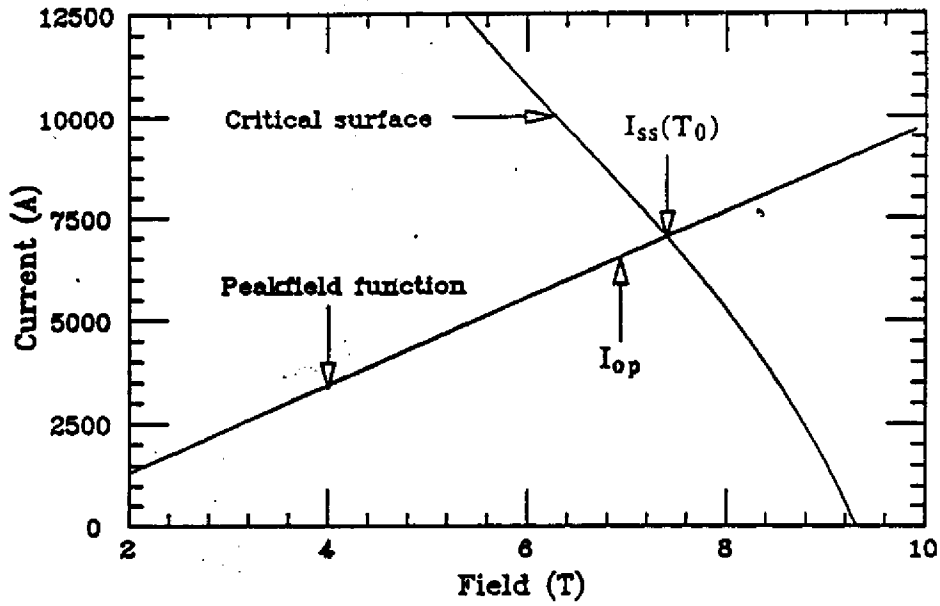


Figure 10. Defining the current margin (in the plane $T = T_0$).

## 5. OPTIMIZING THE QUENCH PERFORMANCE

### 5.1 Operating Margin

As we have seen throughout this paper, an important parameter in the performance of the magnet is the position of the operating point relative to the critical surface. This is called the *operating margin* of the magnet. Since we are in a three-dimensional space, there are many ways to define this margin, depending along which axis the distance from the operating point to the critical surface is measured.

The most commonly used definition is the *current margin*, $m_i$, defined, as illustrated in Figure 10, by considering, in the plane of the operating temperature, the distance from the operating point to the critical surface along the load line. That is

$$m_i = \frac{I_{ss}(T_0) - I_{op}}{I_{ss}(T_0)} \quad , \tag{33}$$

where $I_{op}$ is the operating current. One can also write

$$m_i = 1 - n_{op} \quad , \tag{34}$$

where $n_{op}$ is the fraction of short sample calculated for $I_{op}$.

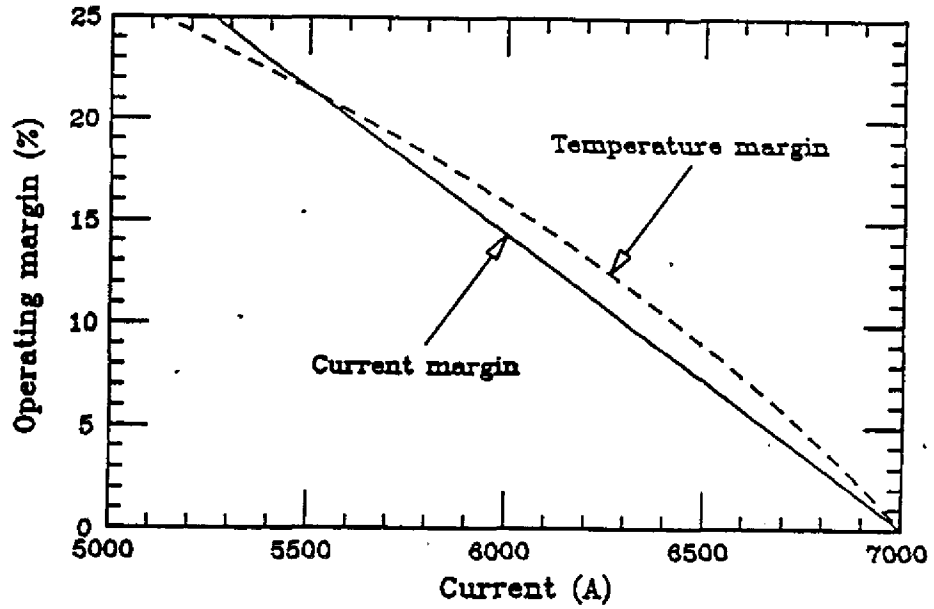


Figure 11. Current margin versus temperature margin ($T_0$ = 4.35 K).

However, as we have seen previously, the training quenches do not occur by crossing the critical surface along the load line, but rather because somewhere in the coil a volume of conductor has seen a temperature increase from $T_0$ to $T_{CI}$. A more suitable parameter to judge the coil stability against the disturbances seems therefore to be the *temperature margin*, $m_t$, defined by

$$m_t = \frac{T_{CI}(I_{op}) - T_0}{T_{CI}(I_{op})} \quad . \tag{35}$$

Figure 11 shows a comparison of these two margins for the actual specifications of the SSC inner-layer conductor, which are listed in Table 1. It appears that, for currents above 5000 A, the current margin is smaller than the temperature margin. From the engineering point of view, $m_i$ therefore imposes tighter constraints than $m_t$, which explains why it is the parameter most often considered in the design studies.

The question that arises now is: what margin value can ensure good magnet reliability? Common sense tells us that the magnet ought not to be operated too close to the critical surface. But what does "too close" mean? And, more generally, what is the relation between $m_i$ and the actual risk of quenching? No answer to these questions can be found directly in the definition of $m_i$. And indeed, the operating margin greatly varies from one project to another: it is about 25% for the HERA dipoles, and about 10% for the SSC dipoles. Of course, more margin means more stability, but on the other hand, it means a bigger magnet or larger conductors, that is, in both cases, more superconductor and, in the end, higher costs. An optimum must therefore be found.

## 5.2 Optimizing the Margin

### 5.2.1 Uncancelable Training

Let us begin from the beginning. The real questions at the root of the problem are: 1) how easy it is to trigger a quench, and 2) what we can best do in building the magnet In other words: 1) what is the size of the disturbances that can trigger a quench?, and 2) what are the mechanical tolerances that can be achieved in building the magnet? Let $\delta$ designate a characteristic size of the *minimum quenching disturbance*, and $t_m$ the *mechanical tolerances*. An adequate criterion to judge the magnet operability seems therefore to compare $\delta$ and $t_m$. A sound magnet will of course be a magnet such that

$$\delta >> t_m \quad , \tag{36}$$

On the other hand, if $\delta$ happens to be of the same order as $t_m$, that is, if the minimum quenching disturbances are of the same size as the mechanical tolerances, there is what I shall call an *uncancelable risk of training*, which will remain during the whole magnet life and can strike at random.

A careful evaluation of $\delta$ and $t_m$ would demand a full investigation of the details of the magnet mechanics, which are discussed elsewhere.[58,104] In this broad presentation, I am more interested by orders of magnitude than by accurate numbers. I shall therefore content myself with simple estimations. In the following, longitudinal refers to a characteristic measured along the conductor or along the axis of the magnet, while radial refers to a characteristic measured in the coil's cross section.

### 5.2.2 Size of the Minimum Quenching Disturbance

In paragraph 4.2, we showed that to trigger a quench a minimum energy $W_{CI}$ has to be deposited on a minimum length $l_{CI}$ of conductor. $l_{CI}$ therefore defines the longitudinal characteristic size of the minimum quenching disturbances. On the other hand, we saw in paragraph 4.3 that training has two main origins, both of mechanical nature: wire motion and epoxy failure. In both cases, we were then able to evaluate a transverse, or radial, characteristic size of the minimum quenching disturbances. Let me resume here the estimation of the radial characteristic size.

Since we are dealing with mechanically-induced quenches, let $E_m$ designate the mechanical energy stored per unit volume of coil. The energy $Q$ that can be released by a volume $V$ of coil is

$$Q = E_m V \quad . \tag{37}$$

Assuming that the energy is entirely consumed in heating the conductor, a quench can only be triggered if

$$Q \geq W_{CI} \quad . \tag{38}$$

The minimum volume of disturbance $V_{min}$ that can trigger a quench is thus

$$V_{min} = \frac{W_{CI}}{E_m} \quad . \tag{39}$$

Let us write $V_{min}$ under the form

$$V_{min} = a\, b\, \delta \quad , \tag{40}$$

where $a$ is the longitudinal characteristic size of the minimum quenching disturbance, and $b$ and $\delta$ are the radial characteristic sizes. As we said earlier, we must have

$$a = l_{CI} \quad . \tag{42}$$

The conductor is a composite structure, but the smallest part of the conductor that can be mechanically affected is a strand. We must therefore have

$$b = d \quad , \tag{43}$$

where $d$ is the strand diameter. Combining Eqs. (39) to (43) shows that

$$\delta = \frac{W_{CI}}{E_m\, l_{CI}\, d} \quad . \tag{44}$$

The last step of our calculations is now to estimate $E_m$. The general expression of the mechanical energy is

$$E_m = \frac{1}{2} \frac{\sigma_{av}^2}{Y_{av}} \quad , \tag{45}$$

where $\sigma_{av}$ is the average azimuthal stress, and $Y_{av}$ is the average young modulus of the coil. (This differs from paragraph 4.3.2.2, where we only considered the Lorentz force, and from paragraph 4.3.3.2, where we only considered the impregnating resin). The young modulus has to be specifically measured on the coil, or on a stack of conductors representative of the coil, and depends on many parameters. In the following we shall take

$$Y_{av} = 10 \text{ GPa} \quad .$$

The stress can be calculated by a computer simulation, or, better yet, it can be directly measured on a working magnet by means of strain gauges, as is currently done on the SSC dipole prototypes.[106] The stress depends of course on the energization current. For the most recent 4-cm aperture, 17-m long SSC dipoles, the stress-current relation can be represented by[6-9]

$$\sigma_{av} = -0.51\, I^2 + 55.4\, 10^6 \qquad \text{(Pa)}. \tag{46}$$

Table 2 presents the results of these calculations for the specified SSC inner-layer conductor, and for the conductors wound in dipole prototypes DD0017 and DD0019. It appears that, for these two magnets, the longitudinal and radial characteristic sizes of the minimum quenching disturbances are respectively 0.5 mm and 150 μm. In order to prevent any mechanically-induced quenches, the part of the coil that sees the highest magnetic field should therefore be mechanically secured with tighter tolerances than these two numbers.

Table 2. Current Margin and Minimum Quenching Disturbance Sizes of SSC Dipole Prototypes at 6500 A and 4.35 K

| | Specifications | DD0017 | DD0019 |
|---|---|---|---|
| $m_i$ (%) | 7.2 | 4.7 | 2.9 |
| $l_{CI}$ (μm) | 633 | 554 | 436 |
| $\delta$ (μm) | 342 | 198 | 122 |

### 5.2.3 Mechanical Tolerances

To make a comparison with the longitudinal and radial characteristics of the minimum quenching disturbance, I should now evaluate the tolerances in theses two directions. However, one can reasonably guess that the most constraining will be the radial tolerances, so I shall therefore limit myself to those.

The radial tolerances can in fact be divided into three terms: 1) the fabrication tolerances, which I shall note $t_f$, 2) the differences in thermal shrinkage between the magnet components during cool down, which I shall note $t_{th}$, and 3) the deformations due to Lorentz forces during energization, which I shall note $t_e$.

The fabrication tolerances that can influence the positioning of the conductor are the degrees of accuracy of the stainless-steel collar size and of the conductor size itself. In the case of the SSC, the specifications are 20 to 30 μm for the collar size, and 15 μm for the conductor width. An estimate of $t_f$ is thus

$$t_f = 40\ \mu m \quad .$$

The differential in shrinkage between stainless steel and copper from room temperature to helium temperature is 0.05%. For a 4-cm aperture coil, like that of the 17-meter SSC dipole prototypes mentioned in this paper

$$t_{th} = 20\ \mu m \quad .$$

The coil deformation during energization is much more complicated to estimate, and needs a computer simulation. For the actual design of the SSC dipole coil at 6500 A, a conservative number is probably

$$t_e = 100\ \mu m \quad .$$

It now remains to add up these three numbers. However, as we mentioned in paragraph 4.3.2.3, the coil is prestressed at room temperature in order to cancel, at least partially, $t_{th}$ and $t_e$. The effectiveness of this cancellation is still open to debate.[58] Let us nonetheless divide $t_{th}$ and $t_e$ by two. We get

$$t_m = 100\ \mu m \quad .$$

Comparing this value with the values of $\delta$ listed in Table 2 shows that, for DD0017 and DD0019, they are of the same order. These magnets were therefore operated in the region of uncancelable training, as is confirmed by the fact that they both exhibited training quenches for currents of about 6500 A.

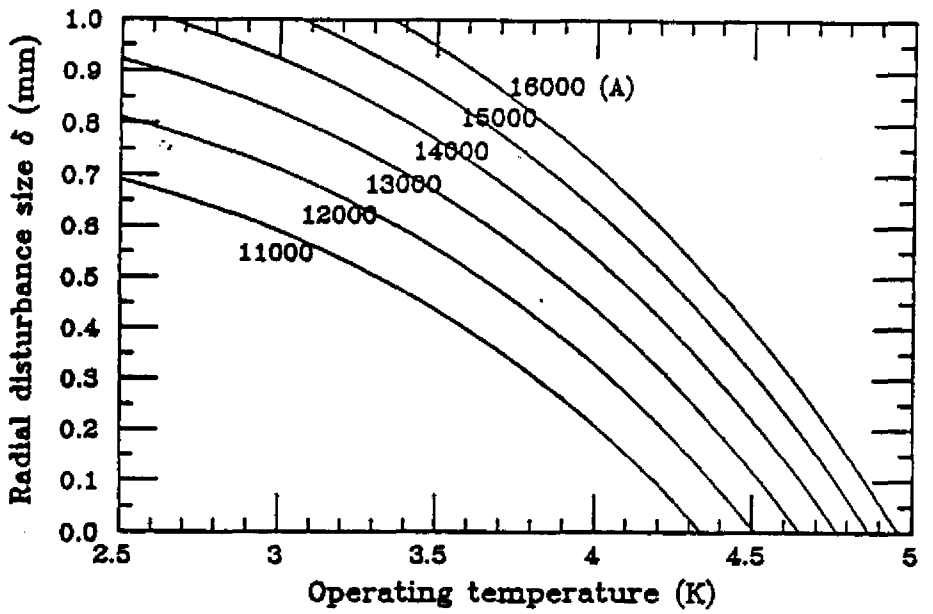


Figure 12. Influence of the operating temperature for various $I_C$(4.2 K, 5 T).

5.2.4 Parameters Influencing $\delta$

According to our criteria, a sound magnet is a magnet verifying Eq. (36). Since there is little hope of improving $t_m$, the main efforts of the magnet designer should be directed towards optimizing $\delta$, that is, towards choosing an operating point for which $\delta$ is well above $t_m$. $\delta$ depends mainly upon three parameters: the operating temperature, $T_0$, the conductor critical current, $I_C$, and the copper-to-superconductor ratio, $r_{CuS}$.

Figure 12 presents a set of plots $\delta = f(T_0)$ for different values of $I_C$(4.2 K,5 T), and for the parameters of the present 4-cm aperture SSC dipole design. As expected, the better the conductor (higher $I_C$), and the lower the temperature, the larger the minimum quenching disturbance is. Also noticeable on this plot is the steepness of the curves for temperatures above 4.2 K. On the other hand, by cooling down the magnet to 3.5 K, an important factor can be gained on $\delta$ — a factor of about five for a critical current of 12000 A. This can be related well to magnet DD0019 testing results, which exhibited some training when operated at 4.35 K, but no quenching when operated at 3.5 K up to currents of 6700-6800 A; lowering the temperature has dramatically increase its $\delta$.

More prudence is needed to study the influence of the copper-to-superconductor ratio, since varying $r_{CuS}$ also affect $I_C$. To make sense of the comparison one parameter has to be kept constant. This can be the critical current density $J_C$ in the filaments. $I_C$ and $J_C$ are of course related by

$$I_C = J_C \frac{A}{1 + r_{CuS}} \quad , \tag{47}$$

where $A$ is the conductor cross-sectional area.

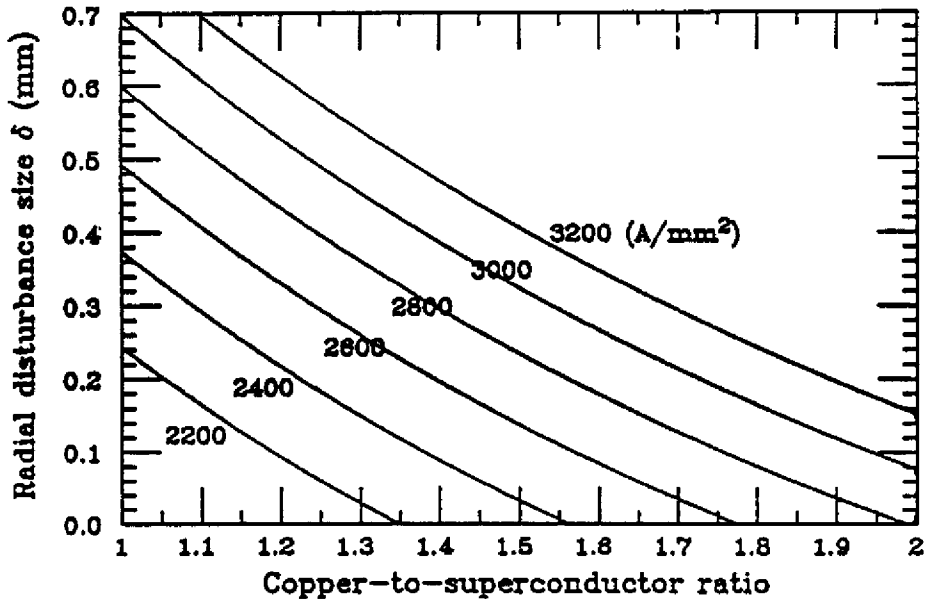


Figure 13. Influence of the copper-to-superconductor ratio for various $J_C$(4.2 K, 5 T) ($T_0$ = 4.35 K).

Figure 13 presents a set of plots $\delta = f(r_{CuS})$ for different values of $J_C$(4.2 K,5 T), and for the parameters of the present 4-cm aperture SSC dipole design. As expected, the higher the overall critical current (that is, at $J_C$ constant, the more superconductor there is), the larger the minimum quenching disturbance is. Nevertheless, the curves are much less steep than in the previous plot. For a critical current of 2750 A/mm$^2$ (which is the value currently achieved in the modern conductors), $\delta$ varies by barely a factor of two when $r_{CuS}$ is changed from 1.3 to 1.6. This can also be related to the test results of the most recent 4-cm aperture, 17-m long SSC dipole prototypes, which, even though they were built with different conductors of different copper-to-superconductor ratios, all exhibited very similar training behavior;[8,9] their $\delta$ are of the same order of magnitude.

5.2.5 Relation Between the Current Margin and $\delta$

To conclude this section I want to show how the previous considerations of $\delta$ can be translated in terms of current margin. Figure 14 shows a plot of $m_i$ = f($\delta$) for different values of $I_C$(4.2 K, 5 T), and for the parameters of the present 4-cm aperture SSC dipole design. The plot shows that a 5% current margin corresponds to a quenching disturbance size of 200 μm, thus very close to the achievable mechanical tolerances; that a 10% margin corresponds to a quenching disturbance size of 500 μm, which may be sufficient according to the early results on magnet DD0019 at 3.5 K, but which needs to be confirmed for more magnets; and that a 25% margin corresponds to a quenching disturbance size of 1 mm, which this time is one order of magnitude larger than the mechanical tolerances.

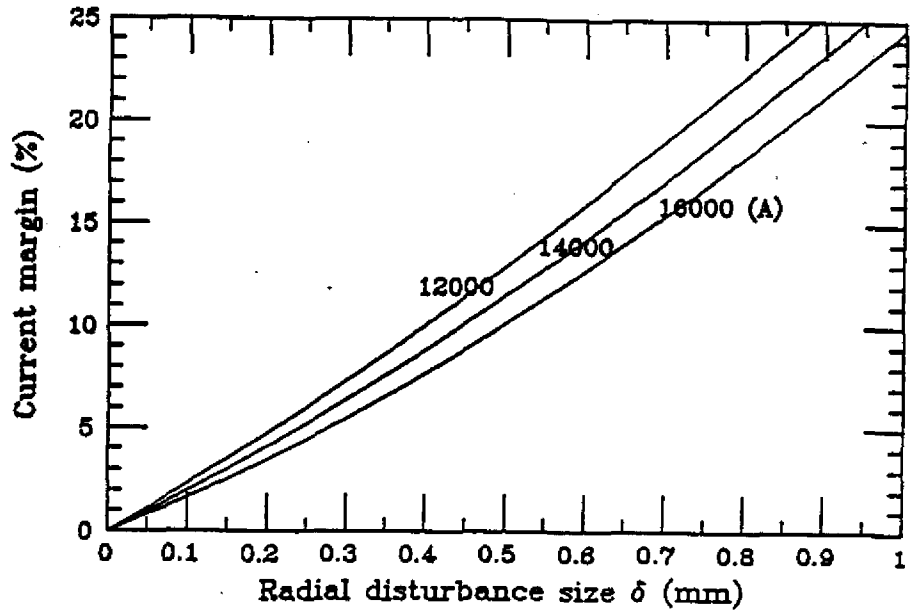


Figure 14. Optimizing the margin for various $I_C$(4.2 K, 5 T) ($T_0$ = 4.35 K).

Deciding which level of current margin is suitable now depends on the magnet builder's taste for challenge. The aim for the SSC is 10%, which has not yet been achieved because the conductor still needs some improvement on the critical current. On the other hand, the designers of HERA had chosen a more conservative approach, with a 25% margin, and have achieved such success that it is now a question of increasing the operating current of the machine.

## 6 CONCLUSION

Quenches can be divided into two categories: conductor-limited and energy-deposited quenches. A conductor-limited quench occurs when the current in the magnet exceeds the capacity of the superconductor; it is characterized by a strong correlation with temperature. An energy-deposited quench occurs when a disturbance releases enough energy to trigger a quench; the main disturbances during magnet energization are frictional movements of the conductor due to increasing Lorentz forces. The current level of the conductor-limited quenches defines the limit of the magnet performance, and can only be surpassed by lowering the operating temperature; the occurrence of a constant current at quench during the magnet testing is called a plateau. Usually it takes a few energy-deposited quenches of increasing currents to reach the plateau; these first few steps are called the magnet's training. The goal in designing a magnet is to be able to energize it and to reliably operate it at the design current without training. This can be achieved by optimizing the magnet's operating margin, that is, by designing and building the magnet in such a way that the sizes of the mechanical disturbances needed to trigger a quench are much larger than the achievable mechanical tolerances.

## ACKNOWLEDGMENTS

The author is deeply indebted to Maury Tigner, who, as head of the SSC Central Design Group, made most of this work possible. I wish to thank Chris Quigg and Roger Coombes for their countless encouragements, and John Tompkins, Robert Schermer, Peter Wanderer, and Jon Zbasnik for many fruitful discussions. I would also like to thank Peter Mazur and the crew of the Fermilab Magnet Test Facility for their unwavering commitment through both the torpor of midday and the coldness of dawn in the Land of Lincoln. I am grateful to Takakazu Shintomi for his support during the redaction of this paper, and to Jared Stark for his insightful comments on the manuscript.

## APPENDIX: MATERIAL PROPERTIES

### 1. Conductor Properties

Throughout the paper, the specific heat per unit volume, the thermal conductivity, and the resistivity in the normal state of the conductor are calculated as

$$C = \frac{r_{CuS}}{1+r_{CuS}} C_{Cu} + \frac{1}{1+r_{CuS}} C_{NbTi} \qquad (\mathrm{Jm^{-3}K^{-1}}),$$

$$k = \frac{r_{CuS}}{1+r_{CuS}} k_{Cu} + \frac{1}{1+r_{CuS}} k_{NbTi} \qquad (\mathrm{Wm^{-1}K^{-1}}),$$

$$\rho = \frac{1+r_{CuS}}{r_{CuS}} \rho_{Cu} \qquad (\Omega\mathrm{m}),$$

where $r_{CuS}$ is the copper-to-superconductor ratio.

### 2. Copper Properties

The copper specific heat and the copper resistivity are computed using the data and the fits provided in references 107 and 108

$$C_{Cu}(T) = 105\, T^{1.2} + 2.4\, T^{3.4} \qquad \text{for } 1 < T < 20 \text{ K},$$

$$\log\left(\frac{C_{Cu}(T)}{8.92\ 10^3}\right) = 1.131 - 9.454\,(\log T) + 12.99\,(\log T)^2 - 5.501\,(\log T)^3 + 0.7637\,(\log T)^4 \qquad \text{for } 4 < T < 300 \text{ K},$$

and

$$\rho_{Cu}(\mathrm{RRR}, T, B) = (1+r)\, \rho_{Cu}(\mathrm{RRR}, T, B=0) \qquad \text{for } 2 < T < 900 \text{ K},$$

where

$$\rho_{Cu}(\mathrm{RRR}, T, B=0) = \rho_0 + \rho_i + \rho_{i0} \quad ,$$

$$\rho_0 = \frac{15.53\ 10^{-9}}{\mathrm{RRR}} \quad ,$$

$$\rho_i = \frac{1.171\ 10^{-17}\ T^{4.49}}{1 + 4.498\ 10^{-7}\ T^{3.35}\ \exp\left(-(50/T)^{6.428}\right)} \quad ,$$

$$\rho_{i0} = 0.4531\ \frac{\rho_0\ \rho_i}{\rho_0 + \rho_i} \quad ,$$

$$\log r = -2.662 + 0.3168 \log s + 0.6229 (\log s)^2 - 0.1839 (\log s)^3 + 0.01827 (\log s)^4 \quad ,$$

$$s = \frac{15.53\ 10^{-9}\ B}{\rho_{Cu}(\mathrm{RRR}, T, B{=}0)} \quad ,$$

RRR is the Residual Resistivity Ratio.

The copper thermal conductivity is computed according to the Wiedeman-Franz law and assuming that the Lorentz constant L is independent of the magnetic field

$$k_{Cu}(\mathrm{RRR}, T, B) = \frac{2.44\ 10^{-8}\ T}{\rho_{Cu}(\mathrm{RRR}, T, B)} \qquad \text{for } T < 10 \text{ K.}$$

3. Niobium-titanium properties

Following reference 109, we write the specific heat of NbTi under the form

$$C_{NbTi}(T, B) = \left(\beta + \frac{3\gamma}{T_C^2}\right) T^3 + \frac{\gamma}{h} B\ T \qquad \text{for } T < T_{CI},$$

and

$$C_{NbTi}(T, B) = \gamma T + \beta T^3 \qquad \text{for } T_{CI} < T < 10 \text{ K},$$

where $\beta$ is the electronic specific heat coefficient, $\gamma$ is the lattice specific heat coeeficient, $T_C$ is the critical temperature at zero field and zero current, and $h$ is a coefficient proportional to the upper critical field at zero Kelvin. (For $T = T_{CI}$, we use the average value of these two expressions.) Measurements of $T_C$, $\beta$, and $\gamma$ for the niobium– 46.5 wt% titanium are provided by reference 110; an estimation of $h$ can be derived from the data of reference 109. With a working density of 6.02 g/cm$^3$ we have

$$T_C = 8.5 \text{ K}, \quad \beta = 16.07 \text{ Jm}^{-3}\text{K}^{-4}, \quad \gamma = 1011.8 \text{ Jm}^{-3}\text{K}^{-2}, \quad h = 10.15 \text{ T}.$$

The thermal conductivity of niobium titanium is assumed to be independent of the magnetic field,[111] and is computed using the fit provided in Reference 112

$$k_{NbTi}(T) = 7.5\ 10^{-3}\ T^{1.85} \qquad \text{for } T < 10 \text{ K.}$$

## REFERENCES


1. A. Devred, M. Chapman, et al., "Quench start localization in full-length SCC R&D dipoles," to appear in the proceedings of the First International Industrial Symposium of the Super Collider, New Orleans, Louisiana, USA, February 8-10, 1989.

2. A. Devred, M. Chapman, et al., "Quench characteristics of full-length SSC R&D dipole magnets," to appear in the proceedings of the 1989 Cryogenic Engineering Conference, Los Angeles, California, USA, July 24-28, 1989.

3. A. Devred, M. Chapman, et al., "Investigation of heater-induced quenches in a full-length SSC R&D dipole," to appear in the proceedings of the 11th International Conference on Magnet Technology, Tsukuba, Ibaraki, Japan, August 28-September 1, 1989.

4. This classification reflects the conclusions of the Magnet Training/Re-Training Working Group held at the SSC Laboratory in September 1989.

5. Credit for the establishment of the criterion is to be given to J. C. Tompkins.

6. J. Tompkins, M. Chapman, et al., "Performance of full-length SSC model dipoles: results from 1988 tests," to appear in the proceedings of the First International Industrial Symposium of the Super Collider, New Orleans, Louisiana, USA, February 8-10, 1989.

7. J. Strait, B. Brown, et al., "Full-length SSC R&D dipole magnet test results," to appear in the proceedings of the 1989 Particle Accelerator Conference, Chicago, Illinois, USA, March 20-23, 1989.

8. C. Goodzeit, P. Wanderer, et al., "Status report on SSC dipole R&D," to appear in the proceedings of the 10th workshop on the INFN Eloisatron Project — New Techniques for Future Accelerators, High Intensity Storage Rings, States and Prospects for Superconducting Magnets — Erice, Italy, October 16-24, 1989.

9. Peter Wanderer, "Performances of SSC R&D dipoles," lecture given at the 1989/1990 US Particle Accelerator School, Brookhaven National Laboratory, Upton, New York, USA, July 29-August 4, 1989, to appear in these proceedings.

10. E. Gregory, lecture given at the 1989/1990 US Particle Accelerator School, Brookhaven National Laboratory, Upton, New York, USA, July 29-August 4, 1989.

11. Courtesy Brookhaven National Laboratory, Upton, New York, USA.

12. M. Garber, W. B. Sampson, et al., "Critical current measurements on superconducting cables," *IEEE Trans. Magn.*, MAG-19 No 3, 1983, p. 720.

13. M. Garber, M. Suenaga, et al., "Critical current studies on fine filamentary NbTi accelerator wires," *Adv. Cryo. Eng. Materials*, 32, 1986, p. 707.

14. G. Morgan and W. B. Sampson, "New coefficients for a $J_C(B,T)$ analytic form," SSC Technical Note No. 79, Accelerator Development Department, Brookhaven National Laboratory, Upton, New York, USA, June 10, 1988.

15. M. A. Green, "Calculating the $J_C$, $B$, $T$ surface for niobium titanium using a reduced-state model," *IEEE Trans. Magn.*, MAG-25 No. 2, 1989, p. 2119.

16. G. Morgan, "A comparison of two analytic forms for the $J_C$ $(T, B)$ surface," Magnet Division Note No. 310-1 (SSC-MD-218), Accelerator Development Department, Brookhaven National Laboratory, Upton, New York, USA, January 6, 1989.

17. M. Garber and W. B. Sampson, "Test methods for cable critical currents and normal state resistance," SSC Technical Note No. 70, Accelerator Development Department, Brookhaven National Laboratory, Upton, New York, USA, March 3, 1988.

18. G. Morgan, "Shaping of magnetic field in beam transport magnets," lecture given at the 1989/1990 US Particle Accelerator School, Brookhaven National Laboratory, Upton, New York, USA, July 29-August 4, 1989, to appear in these proceedings.

19. *Conceptual Design Report of the Superconducting Super Collider*, J. D. Jackson editor, SSC Central Design Group, Lawrence Berkeley Laboratory, Berkeley, California, USA, September 1986.

20 A. P. Martinelli and S. L. Wipf, "Investigation of cryogenic stability and reliability of operation of $Nb_3Sn$ coils in helium gas environment," Proceedings of the 1972 Applied Superconductivity Conference, Annapolis, Maryland, May 1-3, 1972, (IEEE, New York, 1972), p. 331.

21. N. M. Wilson and Y. Iwasa, "Stability of superconductors against localized disturbances of limited magnitude," *Cryogenics*, **18**, 1978, p. 17.

22. S. L. Wipf, "Stability and degradation of superconducting current-carrying devices," Los Alamos Scientific Laboratory Report No. 7275, December 1978.

23. N. M. Wilson, *Superconducting Magnets*, Clarendon Press, Oxford, 1983, p. 79.

24. M. C. M. Cornelissen and C. J. Hoogendoorn, "Thermal stability of superconducting magnets: static criteria," *Cryogenics*, **24**, 1984, p. 669.

25. R. Jayakumar, "Critical energy of superconducting composites," *Cryogenics*, **27**, 1987, p. 421.

26. W. Y. Chen and J. R. Purcell, " Numerical study of normal-zone evolution and stability of composite superconductors," *J. Appl. Phys.*, 49(6), 1978, p. 3546.

27. V. E. Keilin and V. R. Romanovsky, "The dimensionless analysis of the stability of composite superconductors with respect to thermal disturbances," *Cryogenics*, 22, 1982, p. 313.

28. V. R. Romanovskii, "Influence of volume fraction of superconductor on the stability of superconducting composites with respect to thermal disturbances of finite extent," *Cryogenics*, 25, 1985, p. 327.

29. V. R. Romanovskii, "Stability of superconducting composites under thermal disturbances with change in the external magnetic field and the critical temperature of the superconductor," *Cryogenics*, 28, 1988, p. 756.

30. L. Dresner, "Quench energies of potted magnets," *IEEE Trans. Magn.*, Mag-21 No. 2, 1985, p. 392.

31. L. Dresner, "Quench energies of potted magnets III," *Adv. Cryo. Eng.*, 31, 1986, p. 365.

32. G. Reiter, "Response of superconductors to fast heat pulses," *Cryogenics*, 22, 1982, p. 451.

33. A. L. Rakhmanov, "Normal zone initiation in composite superconductors," *Cryogenics*, 23, 1983, p. 487.

34. W. Goll and P. Turowski, "Quenching of technical superconductors by heat and magenetic field pulses," *Cryogenics*, 18, 1978, p. 103.

35. C. Schmidt, "The induction of a propagating normal zone (quench) in a superconductor by local energy release," *Cryogenics*, 18, 1978, p. 605.

36. O. P. Anashkin, V. E. Keilin, and V. V. Lyikov, "Stability of compound superconductors under localized heat pulses," *Cryogenics*, 19, 1979, p. 77.

37. M. J. Supercsynski, "Heat pulses required to quench a potted superconducting magnet," *IEEE Trans. Mag.*, Mag-15 No. 1, 1979, p. 325.

38. D. J. Waltman, M. J. Superczynski, and F. E. McDonald, "Energy pulses required to quench potted superconducting magnets at constant field," *IEEE Trans. Magn.*, Mag-17 No. 1, 1981, p. 1056.

39. A. D. McInturff, W. B. Sampson, et al., "Quench behavior of a superconducting accelerator magnet," *IEEE Trans. Magn.*, Mag-17 No. 1, 1981, p. 432.

40. D. E. Baynham, V. W. Edwards, and N. M. Wilson, "Thermal stability of high current denstty superconducting wires," *IEEE Trans. Magn.*, Mag-17 No. 1, 1981, p. 732.

41. C. A. Scott, "Minimum heat pulse to quench a superconducting magnet," *Cryogenics*, 22, 1982, p. 577.

42. *Proceedings of the workshop on Stability of Superconductors in Helium I and II, Saclay, France, November 16-19, 1981*, edited by Institut International du Froid (Commission A1/2), Paris, France, 1981.

43. L. Dresner, "Superconductor stability, 1983: a review," *Cryogenics*, 24, 1984, p. 283.

44. same as 23, p. 74.

45. H. S. Carslaw and J. C. Jaeger, *Conduction of heat in solids*, Clarendon Press, Oxford, 1959, p. 54.

46. V. E. Keilin, S. L. Kruglov, and S. A. Lelekhov, "The investigation of size effect in superconducting current carrying elements," *Cryogenics*, **19**, 1979, p. 27

47. V. E. Keilin, I. A. Kovalev, and S. L. Kruglov, "Training and degradation of a model superconducting winding depending on cooling conditions and conductor cross-section," *Cryogenics*, **25**, 1985, p. 1985.

48. A. V. Tollestrup, " Care and training of superconducting magnets, " *IEEE Trans. Magn.*, **MAG-17 No. 1**, 1981, p. 863.

49. P. F. Smith, N. M. Wilson, and A. H. Spurway, "IV. DC coil tests," *J. Phys.*, **D3**, 1970, p. 1561.

50. O. Tsukamoto, H. Maeda, and Y. Iwasa, "Microslip-induced degradation in a braided superconductor," *Appl. Phys. Lett.*, **39**(11), 1981, p. 918.

51. R. S. Kensley, H. Maeda and Y. Iwasa, "Transient slip behaviour of metal/insulator pairs at 4.2 K," *Cryogenics*, **21**, 1981, p. 479.

52. H. Maeda, O Tsukamoto, and Y. Iwasa, "The mechanism of frictional motion and its effects at 4.2 K in superconducting magnet winding models," *Cryogenics*, **22**, 1982, p. 287.

53. O. Tsukamoto and Y. Iwasa, "Mechanical disturbances in Rutherford type and braid conductors," *IEEE Trans. Magn.*, **Mag-19 No. 3**, 1983, p. 443.

54. T. Nishiura, S. Owaki, et al., "Frictional behavior in superconducting coil," *IEEE Trans. Magn.*, **Mag-21 No.2**, 1985, p. 384.

55. O. Tsukamoto, T. Takao, and S. Honjoh, "Estimating the size of disturbances due to conductor motion in superconducting windings," *IEEE Trans. Magn.*, **Mag-24 No.2**, 1988, p. 1182.

56. O. Tsukamoto, T. Takao, and S. Honjo, "Quantification of disturbance energy due to conductor motion and stability anaylsis of superconducting composite wire," *IEEE Trans. Magn.*, **Mag-25 No.2**, 1989, p. 1713.

57. O. P. Anashkin, A. L. Glytenko, et al., "Effect of the axial component of the Lorentz froce on training and degradation of superconducting coils," *Cryogenics*, **22**, 1982, p. 94.

58. R. I. Schermer, lecture given at the 1989/1990 US Particle Accelerator School, Brookhaven National Laboratory, Upton, New York, USA, July 29-August 4, 1989.

59. T. Shintomi, A. Terashima, and H. Hirabayashi, "Development of superconducting dipole magnet with ideal arch structure using large keystone angle cable," to appear in the proceedings of the 11th International Conference on Magnet Technology, Tsukuba, Japan, August 28-September 1, 1989.

60. T. Shintomi, A. Terashima, et al., "Development of superconducting dipole magnet for large hadron accelerator," *Proceedings of the 42nd Meeting on Cryogenics and Superconductivity, Hiroshima, Japan, December 11-13, 1989*, p. 68 (in Japanese).

61. V. W. Edwards, C. A. Scott, and N. M. Wilson, "The control of 'training' in 'racetrack' shaped superconducting magnets," *IEEE Trans. Magn.*, **Mag-11 No.2**, 1975, p. 532.

62. V. W. Edwards and N. M. Wilson, "The effect of adhesion between turns on the training of superconductings magnets," *Cryogenics*, **18**, 1978, p. 423.

63. J. W. Ekin, R. E. Schramm, and A. F. Clark, "Effect of strain on epoxy-impregnated superconducting composites, " *Non Metallic Materials and Composites at Low Temperatures*, Plenum Press, New York, 1979, p. 301.

64. H. Maeda and Y. Iwasa, "Heat generation from epoxy cracks and bond failures, " *Cryogenics*, **22**, 1982, p. 473.

65. Y. Yasaka and Y. Iwasa, "Stress-induced epoxy cracking and energy release at 4.2 K in epoxy-coated superconducting wires," *Cryogenics*, **24**, 1984, p. 423.

66. O. Tsukamoto and Y. Iwasa, "Epoxy cracking in the epoxy impregnated winding: nonuniform dissipation of stress energy in a wire-epoxy matrix model," *IEEE Trans. Magn.*, **Mag-21 No.2**, 1985, p. 377.

67. G. Hartwig and S. Knaak, "Fibre-epoxy composites at low temperatures," *Cryogenics*, **24**, 1984, p. 639.

68. D. A. Wigley, *Mechanical Properties of Materials at Low Temperatures*, Plenum Press, New York, 1971, p. 111.

69. P. F. Smith and B Colyer, "A solution to the 'training' problem in superconducting magnets," *Cryogenics*, **15**, 1975, p. 201.

70. J. W. Ekin, R. E. Schramm, and M. J. Superczynski, "Training of epoxy-impregnated superconductor windings," *Adv. Cryo. Eng. Materials*, **26**, 1980, p. 677.

71. J. W. Ekin, E. S. Pittman, et al., "Training studies of epoxy-impregnated superconductor windings," *Adv. Cryo. Eng. Materials*, **28**, 1982, p. 719.

72. J. W. Ekin, E. S. Pittman, et al., "Training studies of epoxy-impregnated superconductor windings, part III: epoxies, conductor insulations and copper ratio," *Adv. Cryo. Eng. Materials*, **30**, 1984, p. 977.

73. Y. Iwasa, "Experimental and theoretical investigation of mechanical disturbances in epoxy-impregnated superconducting coils. 1. General introduction," *Cryogenics*, **25**, 1985, p. 304.

74. E. S. Bobrov, J. E. C. Williams, and Y. Iwasa, "Experimental and theoretical investigation of mechanical disturbances in epoxy-impregnated superconducting coils. 2. Shear-stress-induced epoxy fracture as the principal source of premature quenches and training – theoritical analysis," *Cryogenics*, **25**, 1985, p. 307.

75. Y. Iwasa, E. S. Bobrov, et al., "Experimental and theoretical investigation of mechanical disturbances in epoxy-impregnated superconducting coils. 3. Fracture-induced premature quenches," *Cryogenics*, **25**, 1985, p. 317.

76. H. Fujita, T. Takaghi, and Y. Iwasa, "Experimental and theoretical investigation of mechanical disturbances in epoxy-impregnated superconducting coils. 4. Prequench cracks and frictional motion," *Cryogenics*, **25**, 1985, p. 323.

77. T. Yamashita, S. Nishijima, et al., "Effect of mechanical disturbances on stability of impregnated windings," *IEEE Trans. Magn.*, **MAG-24 No.2**, 1988, p. 1186.

78. T. Yamashita, S. Nishijima, et al., "Instabilities of impregnated windings induced by epoxy craking," *IEEE Trans. Magn.*, **MAG-25 No.2**, 1989, p. 1524.

79. C. Schmidt, and G. Pasztor, "Superconductors under dynamic mechanical stress," *IEEE Trans. Magn.*, MAG-13 No. 1, 1977, p. 116.

80. O. P. Anashkin, V. A. Varlakhin, et al., "Experimental investigation of training and degradation in superconducting magnet system (SMS)," *IEEE Trans. Magn.*, **Mag-13 No. 1**, 1977, p. 673.

81. A. K. Gosh, M. Garber, et al., "Training in test samples of superconducting cables for accelerator magnets," *IEEE Trans, Magn.*, **Mag-25 No. 2**, 1989, p. 1831.

82. G. Pasztor and C. Schmidt, "Dynamic stress effects in technical superconductors and the 'training' problem of superconducting magnets, "*J. Appl. Phys.*, **49**(2), 1978, p. 886.

83. H. Brechna and P. Turowski, "Training and degradation phenomena in superconducting magnets," *Proceedings of the 6th International Conference on Magnet Technology, Bratislava, Czechoslovakia, August 29-September 2, 1977*, p. 597.

84. R. G. Mints and A. L. Rakhmanov, "Critical state stability in type-II superconductors and superconducting-normal-metal composites," *Review of Modern Physics*, **53**(3), 1981, p. 551.

85. I. L. Maksimov, R. G. Mints, and A. L. Rakhmanov, "Quenching stress, quenching current and plastic yield strain in superconductors," *Cryogenics*, **21**, 1981, p. 715.

86. C. H. Dustman, and H. Köfler, "An attempt to reduce training," *Cryogenics*, **17**, 1977, p. 667.

87. C. Schmidt and B. Turck, "A cure against 'training' of superconductings," *Cryogenics*, **17**, 1977, p. 695.

88 H. Nomura, K. Takahisa, and T. Sakai, "Acoustic emission from superconducting magnets, " *Cryogenics*, **17**, 1977, p 471.

89. P. Turowski, "Acoustic emission and flux jump phenomena during the training of superconducting magnets," *Proceedings of the 6th International Conference on Magnet Technology, Bratislava, Czechoslovakia, August 29-September 2, 1977*, p. 648.

90. G. Pasztor, and C. Schmidt, "Acoustic emisson from NbTi superconductors during flux jump," *Cryogenics*, **19**, 1979, p. 608.

91. H. Nomura, M. N. L. Sinclair, and Y. Iwasa, "Acoustic emission in a composite copper NbTi conductor," *Cryogenics*, **20**, 1980, p. 283.

92. M. Pappe, "Acoustic emission in superconducting magnets," *IEEE Trans. Magn.*, Mag-17 No. 5, 1981, p. 2082.

93. O. Tsukamoto, M. W. Sinclair, et al., "Origins of acoustic emission in superconducting wires," *Appl. Phys. Lett.*, **38** (9), 1981, p. 718.

94. O. Tsukamoto, J. F. Maguire, et al., "Identification of quench origins in a superconductor with acoustic emission and voltage measurements, " *App. Phys. Lett.*, **39** (2), 1981, p. 172.

95. O. Tsukamoto, and Y. Iwasa, "Sources of acoustic emission in superconducting magnets," *J. Appl. Phys.*, **54** (2), 1983, p. 997.

96. M. Pappe, "Discussion of acoustic emission of a superconducting solenoid," *IEEE Trans. Magn.*, MAG-19 No. 3, 1983, p. 1086.

97. A. L. Rakhamanov, "Acoustic emission from superconductors due to the normal transition," *Cryogenics*, **25**, 1985, p. 19.

98. S. Nishijima, H. Iwasaki, and T. Okada, "Study of disturbances in superconducting magnets by acoustic emission method," *IEEE Trans. Magn.*, **Mag-21 No. 2**, 1985, p. 388.

99. Written with the help of T. Ogitsu.

100. K. Tsuchiya, H. Hosoyama, et al., "A prototype superconducting insertion quadrupole magnet for Tristan, " *Adv. Cryo. Eng.*, **31**, 1986, p. 173.

101. R. S. Kensley, K. Yoshida, et al., "Acoustic monitoring of the cluster test facility 20 MJ magnet system: a record of disturbance emission and training," *Cryogenics*, **23**, 1983, p. 17.

102. J. Lore, N. Tamada, et al., "Acoustic emission monitoring results from the MFTF magnets," *Cryogenics*, 24, 1984, p. 201.

103. O. O. Ige, A. D. MacInturff, and Y. Iwasa, "Acoustic emission monitoring results from a Fermi dipole, " *Cryogenics*, 26, 1986, p. 131.

104. J. Peoples, "Status of the SSC superconducting magnet program," *IEEE Trans. Magn.*, Mag-25 No. 2, 1989, p. 1444.

105. J. Strait, B. C. Brown, et al., "Tests of full scale SSC R&D dipole magnets," *IEEE Trans. Magn.*, Mag-25 No. 2, 1989, p. 1455.

106. C. L. Goodzeit, M. D. Anerella, and G. L. Ganetis, "Measurement of internal forces in superconducting magnets with strain gauge transducers", *IEEE Trans. Magn.*, Mag-25 No. 2, 1989, p. 1463.

107. *Handbook on Materials for Superconducting Machinery*, National Bureau of Standards, Boulder, Colorado, USA, 1974.

108. N. G. Simon and R. P. Reed, preliminary draft of "Cryogenic properties of copper and copper alloy," National Bureau of Standards, Boulder, Colorado, USA, March 1987.

109. S. A. Erold, J. R. Miller, and L. Dresner, "The specific heat of NbTi from 0 to 7 T between 4.2 K and 20 K," *Adv, Cryo. Eng. Materials*, 28, 1982, p. 601.

110. E. W. Collings, K. R. Marken, et al.,"Low temperature specific heat and magnetic susceptibility of NbTi and NbTiMn alloys," to appear in the proceedings of the 1989 Cryogenic Engineering Conference, Los Angeles, California, USA, July 24–28, 1989.

111. E. I. Dyachkov, R. Herzog, et al., "Thermal conductivity and electrical resistivity of Nb-Ti (HT-50) as a function of temperature and magnetic field," *Cryogenics*, 21, 1981, p. 47.

112. C. Schmidt, "Simple method to measure the thermal conductivity of technical superconductors, e.g., NbTi," *Rev. Sci. Instrum.*, 50(4), 1979, p. 454.